Draft version June 27, 2014
Preprint typeset using LaTeX style emulateapj v. 5/2/11

arXiv:1406.6982v1 [astro-ph.GA] 26 Jun 2014

SEARCHING FOR DIFFUSE LIGHT IN THE M96 GALAXY GROUP

Aaron E. Watkins[1], J. Christopher Mihos[1], Paul Harding[1], John J. Feldmeier[2]

Draft version June 27, 2014

ABSTRACT

We present deep, wide-field imaging of the M96 galaxy group (also known as the Leo I Group). Down to surface brightness limits of $\mu_B = 30.1$ and $\mu_V = 29.5$, we find no diffuse, large-scale optical counterpart to the "Leo Ring", an extended HI ring surrounding the central elliptical M105 (NGC 3379). However, we do find a number of extremely low surface-brightness ($\mu_B \gtrsim 29$) small-scale streamlike features, possibly tidal in origin, two of which may be associated with the Ring. In addition we present detailed surface photometry of each of the group's most massive members – M105, NGC 3384, M96 (NGC 3368), and M95 (NGC 3351) – out to large radius and low surface brightness, where we search for signatures of interaction and accretion events. We find that the outer isophotes of both M105 and M95 appear almost completely undisturbed, in contrast to NGC 3384 which shows a system of diffuse shells indicative of a recent minor merger. We also find photometric evidence that M96 is accreting gas from the HI ring, in agreement with HI data. In general, however, interaction signatures in the M96 Group are extremely subtle for a group environment, and provide some tension with interaction scenarios for the formation of the Leo HI Ring. The lack of a significant component of diffuse intragroup starlight in the M96 Group is consistent with its status as a loose galaxy group in which encounters are relatively mild and infrequent.

Subject headings: galaxies: elliptical – galaxies: groups: individual(Leo I) – galaxies: interactions – galaxies: stellar content – galaxies: structure

1. INTRODUCTION

In the current ΛCDM cosmological paradigm, massive galaxies form hierarchically over time, via the continual accretion of smaller objects (Searle & Zinn 1978; Davis et al. 1985; Frenk et al 1988; White & Frenk 1991; Jenkins et al. 2001; Springel et al. 2005). Massive galaxies may interact with one another as well, leaving behind readily observable signatures in the form of tidal streams or drastic changes in morphology, stellar populations, and kinematics (e.g., Arp 1966; Toomre & Toomre 1972; Toomre 1977; Hernquist 1992; Barnes 1992, 2002). Even after the initial construction of galaxies has ended, however, cosmological simulations indicate that there should remain a wealth of low-mass satellites that continue to interact with the parent galaxy over time (e.g., Frenk et al 1988; Gelb & Bertschinger 1994; Springel et al. 2005, 2008). Observations of the Local Group indeed show a number of low-luminosity satellites around the Milky Way and M31 (Hodge 1971; Feitzinger & Galinski 1985; Mateo 1998; Belokurov et al. 2006; Weisz et al. 2011; McConnachie 2012), lending credence to the idea. However, important discrepancies between theory and observation remain, such as the 'missing satellites problem' (Klypin et al. 1999; Moore et al. 1999), demonstrating the importance of continuing to test the theory observationally in a variety of ways.

Probing the low surface brightness outskirts of galaxies via deep surface photometry provides one such observational test. Under proposed "inside-out" galaxy formation models (Matteucci & François 1989; Bullock & Johnston 2005; Naab & Ostriker 2006; Hopkins et al. 2009; van Dokkum et al. 2010; Kauffmann et al. 2012), even apparently undisturbed galaxies should show signs of recent accretions or interactions in subtle ways in their outskirts, where restoring forces are low and dynamical times are long. Morphological signatures of accretion such as tidal features, warps, and disk asymmetries (Toomre & Toomre 1972; Bullock & Johnston 2005; Martínez-Delgado et al. 2010) may trace the record of past encounters, while changes in the structural properties and stellar populations of the outer disk can be probed via quantitative photometry and color profiles (e.g. van der Kruit 1979; Pohlen et al. 2002; Trujillo et al. 2009; Mihos et al. 2013a). Finding and categorizing such signatures thus becomes an important step in constraining theories of galaxy formation.

Unfortunately, the extended outskirts of galaxies are extremely dim and diffuse. However, with the advent of deep wide-field imaging techniques, over the past decade a wide variety of faint tidal features have been identified around nearby galaxies. These features span a wide range of morphologies, from loops, plumes, and shells (Forbes et al. 2003; Martínez-Delgado et al. 2008, 2009, 2010; Atkinson et al. 2013; Mihos et al. 2013a) to extended streams, diffuse stellar halos, and large-scale intracluster light (Uson et al. 1991; Scheick & Kuhn 1994; Gonzalez et al. 2000; Feldmeier et al. 2004; Adami et al. 2005; Mihos et al. 2005; Rudick 2010b). Gaseous accretion events also appear to influence the properties of disks (Sancisi et al. 2008), fueling new star formation in their low density outskirts and driving the formation of extended ultraviolet (XUV) disks (Thilker et al. 2005; Gil de Paz et al. 2005; Thilker et al. 2007; Lemonias et al. 2011). This extended star formation will in turn affect the age and metallicity distributions, and hence the colors, of the underlying stellar populations in these regions. Meanwhile, internal processes within disks may scatter stars outwards, again resulting in changes in the structure and stellar content of the outer disk (Sellwood & Binney 2002; Debattista et al. 2006; Roskar et al. 2008a,b).

Local environment also must play a role in the accretion history of galaxies and the evolution of their outer regions.

[1] Department of Astronomy, Case Western Reserve University, Cleveland, OH 44106, USA
[2] Department of Physics and Astronomy, Youngstown State University, Youngstown, OH 44555, USA

In massive clusters, for example, frequent and rapid interactions between galaxies tend to produce plumes and streams of starlight, which are shredded over time by interactions within the cluster potential to form the more diffuse intracluster light (ICL) seen in clusters such as Virgo (Rudick et al. 2009). In group environments, where the velocity dispersions are generally lower, slow encounters lead to strong dynamical friction and rapid merging (Hickson et al. 1977; Barnes 1989; Taranu et al. 2013). Contrary to cluster environments, then, galaxies in groups may exhibit long-lived accretion shells or tidal tails in their outskirts (e.g., Quinn 1984; Hernquist & Quinn 1987; Law et al. 2005). Meanwhile, the low density environment around isolated field galaxies should lead to fewer recent interactions and accentuate secular evolution processes that are internal to galaxies (e.g. Kraljic et al. 2012). A complete survey of the processes that shape galaxies thus requires an investigation across all environments.

Of particular interest is the group environment, the most common environment for galaxies to reside. Intragroup starlight (IGL) in loose groups[3] is of significant interest across many studies of galaxy and galaxy cluster evolution. The fraction of baryons within galaxy groups and clusters constrains models of star formation and cluster assembly, and there is strong evidence that the amount of intragroup and intracluster starlight may be a significant contributor to the baryon fraction of these systems (e.g. Gonzalez et al. 2013; Budzynski et al. 2014). The loose group environment may also dynamically "preprocess" galaxies that later fall into galaxy clusters and produce ICL (Mihos 2004), and substructure within the diffuse IGL should trace this process in dynamically evolving galaxy groups.

However, the mean fraction of stars in an IGL component, and how that fraction varies with group/cluster mass, is substantially uncertain. Theoretical studies give conflicting results: some studies have found relatively constant mean IGL/ICL fractions with group/cluster mass, but with large intrinsic scatter (e.g. Sommer-Larsen et al. 2005; Sommer-Larsen 2006; Monaco et al. 2006; Henriques & Thomas 2010; Puchwein et al. 2010; Guo et al. 2011; Contini et al. 2014). Other theoretical studies have found that the mean IGL/ICL fraction (sometimes generalized as the intrahalo stellar fraction; IHL) systematically increases with group/cluster mass (e.g. Murante et al. 2007; Purcell et al. 2008; Watson et al. 2012).

Observationally, wide-field imaging studies of $0.01 < z < 0.4$ galaxy clusters over a large range of cluster mass have also found different behaviors for the IGL/ICL fraction as a function of cluster mass (e.g. Lin & Mohr 2004; Zibetti et al. 2005; Gonzalez et al. 2007, 2013; Budzynski et al. 2014). Studies of nearby individual loose galaxy groups searching for individual intragroup stars also have mixed results. Observational searches for intragroup red giant stars and intragroup planetary nebulae have generally found very small fractions of IGL ($< 2\%$; e.g. Castro-Rodríguez et al. 2003; Feldmeier et al. 2004; Durrell et al. 2004). Usually, these surveys only observe a portion of the galaxy group, and if the IGL has an uneven spatial distribution (e.g. Sommer-Larsen 2006), the IGL fractions found may not be reflective of the entire group. However, in stark contrast, McGee & Balogh (2010) have estimated that $47\%^{+16}_{-15}$ of the stellar mass in galaxy groups is in the IGL component through detections of spectroscopically confirmed hostless intragroup SNe Ia that were within the Sloan Digital Sky Survey (SDSS; York et al. 2000) SN survey.

To improve this situation, more searches for IGL need to be undertaken in galaxy groups over a large range of mass. The M96 Group (sometimes referred to as the Leo I Group), shown in Figure 1, helps serve this purpose well. It is the nearest loose group[4] that contains both early and late type massive galaxies (de Vaucouleurs 1975), and hosts a rather unusual feature – a roughly 200 kiloparsec diameter broken ring of neutral hydrogen, first discovered by Schneider et al. (1983). This ring is fairly diffuse; from Arecibo data, column densities range from 6.4×10^{19} cm^{-2} to as low as 2×10^{18} cm^{-2} (Schneider et al. 1989), although smaller clumps with densities of roughly 4×10^{20} cm^{-2} were also detected using the Very Large Array (Schneider et al. 1986). These higher density clumps appear to be confined to the southernmost portion of the ring, and include a bridge-like feature apparently connecting the ring to M96 (NGC 3368), the most massive spiral galaxy in the group. Two other galaxies – the E1 galaxy M105 (NGC 3379) and the S0 galaxy NGC 3384 – appear to lie near the center of the ring, implying some relation between these three galaxies and the intergalactic HI. A fourth galaxy, the barred spiral M95 (NGC 3351), is associated with the group as well, but due to its relatively large projected separation may not be associated with the ring complex itself. The group also lies near in the sky ($\sim8^\circ$ away) and at a somewhat similar distance to the M66 Group, leading to speculation that the two groups are actually each part of a larger complex of galaxies (Stierwalt et al. 2009).

The origin of the Leo HI Ring is still under debate. Kinematics gleaned from the HI observations show that it appears to be well-modeled by an elliptical orbit with a focus at the luminosity-weighted centroid of NGC 3384 and M105 (Schneider 1985). The rotational period of this model orbit is approximately 4 Gyr, and if the Ring is primordial, this period presents a rough lower limit on its age (see Schneider 1985). The apparent lack of associated starlight and star formation supports this primordial origin hypothesis (Pierce & Tully 1985; Schneider et al. 1989; Donahue et al. 1995), as does the similarity between the radial velocities of the Ring and the galaxies within the group, both of which trend higher in the northwest and lower in the southeast (Schneider 1985). Additionally, Sil'chenko et al. (2003) argue that circumnuclear stellar and gaseous disks in NGC 3384, M96, and M105 show ages and kinematics consistent with accretion from the Ring taking place on gigayear timescales, which may rule out a more recent formation scenario. Of course, crossing times in the group are much shorter than 4 Gyr (Pierce & Tully 1985), which poses problems for the stability of the ring – maintaining its shape would require a shepherding mechanism, presumably by M96 (Schneider 1985) – and the only galaxy in the group whose disk appears aligned with the Ring is NGC 3384, unusual if all of the galaxies formed from a single rotating cloud.

An alternative hypothesis was proposed by Rood & Williams (1984), involving the collision of two spiral galax-

[3] Because of their irregular nature, a precise definition of a 'loose group' is elusive. However, characteristic properties are often adopted to classify them, such as a small number of luminous galaxies within a 0.5 Mpc radius and a velocity spread of ~350 km/s (see, e.g., de Vaucouleurs 1975; Geller & Huchra 1983; Maia et al. 1998). Leo I has been classified as a group using these criteria by de Vaucouleurs (1975), Huchra & Geller (1982), and Tully (1987).

[4] We adopt a distance of 11 Mpc for the M96 Group (Graham et al. 1997); at this distance, $1'$ corresponds to 3.2 kpc.

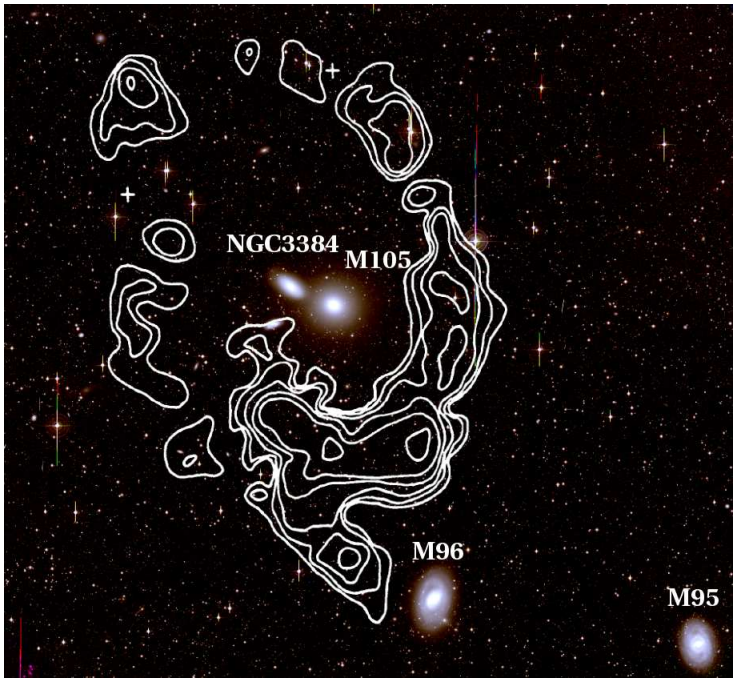

Figure 1. False-color image of the M96 Group, made from a composite of our B and V mosaics. The four largest group members are labeled; the small spiral galaxy south of NGC 3384 is NGC 3389 and is most likely part of a separate group called Leo II, roughly 10 Mpc behind the M96 Group (Stierwalt et al. 2009, and references therein). HI contours from Schneider (1989) are overlaid in white. The image is $1.8° \times 1.8°$ (350×350 kpc^2). North is up and east is to the left.

ies. Under this model, the two galaxies collided nearly head-on, stripping most of the gas from one of the galaxies and producing an expanding density wave much like that proposed to explain the morphology of ring galaxies (e.g., Lynds & Toomre 1976; Gerber et al. 1992; Mazzei et al. 1995; Berentzen et al. 2003). A more recent simulation by Michel-Dansac et al. (2010) managed to reproduce qualitatively all of the important features of the Ring (the annular shape, the apparent rotation, the bridge-like feature described above, and the lack of an apparent visible light counterpart). The simulation collided two gaseous disk galaxies, one of which transformed into an S0: a good facsimile of M96 and NGC 3384. In yet another scenario, the total disruption of a gas-rich, low surface brightness (LSB) galaxy would also leave behind an HI ring with the LSB galaxy's stellar disk completely unaffected (Bekki et al. 2005). In general, the main problem to solve in a collisional hypothesis is to reproduce the apparent lack of optical light associated with the ring, as slow encounters in the loose group environment should be effective at liberating stellar material from the galaxies as well.

To date, neither the primordial origin nor the collisional hypothesis for forming the Leo Ring has been confirmed. No extended diffuse starlight has been found associated with the HI ring; the only known stellar counterpart to the Ring is that discovered by Thilker et al. (2009) in the form of three small far- and near-ultraviolet sources located within the ring's highest density HI complexes (as measured by Schneider et al. 1986). An optical counterpart to at least one of these clumps was later found by Michel-Dansac et al. (2010), with a measured color of $g' - r' = 0.2$, indicative again of a young stellar population. The presence of these clumps thus raises the intriguing possibility that these stars represent the youngest (and therefore brightest) component of an underlying (and as-yet undetected) diffuse stellar counterpart to the ring. All of this makes the M96 Group a particularly intriguing target in a search for the low surface brightness signatures of historical encounters.

This paper presents deep surface photometry of the M96 Group, conducted using Case Western Reserve University's Burrell Schmidt telescope on Kitt Peak and taken as part of an ongoing project to study the outskirts of nearby galaxies across a range of environments. Our deep imaging, covering approximately nine square degrees in two filters, probes the diffuse outskirts of the group members and the Leo Ring down to a surface brightness of $\mu_V \sim 29.5$, with reliable $B-V$ colors down to $\mu_V \sim 28.0$. We use the data to search for diffuse light in the Leo Ring that may trace any past interaction events, as well as to study the structure and stellar populations in the outer disks and halos of the group galaxies.

2. OBSERVATIONS AND DATA REDUCTION

The full description of our observational and data reduction techniques can be found in Rudick et al. (2010a) and Mihos et al. (2013a), however, for the sake of clarity, we describe the most important details here, along with any notable changes to the procedure.

2.1. *Observations*

We observed the M96 Group using the 0.6/0.9m CWRU Burrell Schmidt telescope located at Kitt Peak National Observatory. The telescope has a $1.65° \times 1.65°$ field of view and images onto a 4096×4096 STA0500A CCD[5] for a pixel scale of $1.45''$ pixel^{-1}. We observed in two filters: a modified Johnson B (Spring 2012) and Washington M (Spring 2013). We used Washington M as a substitute for Johnson V, as it covers a similar bandpass but avoids night sky airglow emission lines (Feldmeier et al. 2002); thus, as Washington M is slightly bluer than Johnson V, we used a modified B filter which is 200 Å bluer than standard Johnson B in order to maintain a comparable spectral baseline. For the actual analysis, we

[5] The CCD was backside processed at the University of Arizona Imaging Technology Laboratory.

converted our magnitudes to standard Johnson B and V using observations of Landolt (1992) standard fields. We took data only on moonless photometric nights, although it should be noted that Mars was less than 3° from our target fields during part of the Spring 2012 run and hence may have contributed some low-level scattered light.

Along with target pointings, we also observed offset sky pointings to construct a night sky flat. To minimize uncertainties in the final flat due to changes in sky conditions and telescope flexure, we kept the telescope oriented at roughly the same pointing for flat- field and object exposures by alternating between the two. We dithered individual target exposures randomly by up to half a degree to increase the imaging area and reduce artifacts due to scattered light and large-scale flat fielding errors. Exposure times were 1200 seconds in B (resulting in sky levels of 700 – 900 ADU pixel^{-1}) and 900 seconds in M (1200 – 1400 ADU pixel^{-1}). Our final B and V mosaics contain 41 exposures each, with roughly 30 accompanying blank sky frames per band taken between 0.25 – 1 hr in right ascension and 1 – 4° in declination from the M96 Group. However, we note that the final flat field was produced using blank skies near every object we imaged during the course of this project, for a total of ∼100 frames in B and ∼120 in V (discussed in more detail below). Our total on-target exposure time in the M96 Group is 13.7 hours in B and 10.25 hours in V, although the time spent in each part of the mosaic varies due to dithering across the group's large angular size ($\sim 3^\circ \times 3^\circ$).

2.2. *Data Reduction*

For each frame, we applied an overscan correction and subtracted a nightly mean bias frame using IRAF[6]. We applied no crosstalk corrections; close examination of the images revealed that any visible crosstalk was at such low levels, such a correction was unnecessary. We also corrected each year's data for nonlinear chip response in each quadrant of the CCD using a 4^{th} order polynomial correction. Finally, we applied a world coordinate system to each image to construct the final mosaic.

After a preliminary flat-field correction, we derived a photometric zeropoint for each target frame (directly correcting for airmass effects) using SDSS stars as standards, converted from *ugriz* to Johnson B and V using the conversion formula given by Lupton (2005). We excluded stars outside of the color range $B-V = 0$ to 1.5 from the fit (Ivezić et al. 2007). To derive each filter's color term, we took exposures of Landolt standard star fields (Landolt 1992) at varying exposure times at the beginning and end of each night, as using Landolt stars avoids any error inherent in a color conversion formula. From our final mosaics, we were able to recover converted SDSS magnitudes to $\sigma_V = 0.03$ mag and B-V colors to $\sigma_{B-V} = 0.05$, using SDSS stars in the magnitude range V = 15-17 and the color range $B - V$ = 0.0-1.5.

After applying zeropoints, and assuming that the night sky has an average B-V color near unity (Krisciunas 1997; Patat 2003), we measured sky brightnesses from μ_B = 22.32 to 21.89 and from μ_V = 21.72 to 21.43. These values changed throughout the course of a night, as well as from night to night due to changes in solar output, lunar phase, and atmospheric conditions (e.g. dust, humidity, etc.). However, the faintest sky brightness measurement can act as a useful secondary check, by comparing our measured sky brightnesses to previously measured values under similar conditions. To measure the actual sky brightness, we first removed our airmass corrections of 0.27 mag and 0.16 mag in B and V, respectively, since the source of the sky brightness is mostly within the Earth's atmosphere. We then compared our faintest values (μ_V = 21.88, μ_B = 22.59) to the empirical relation of Krisciunas (1997, see their equation 5), which correlates the average observed night sky brightness to the 10.7cm solar flux. Taking the monthly 10.7cm values from the Dominion Radio Astrophysical Observatory[7], we find an adjusted expected sky brightness of $\mu_V = 21.75 \pm 0.06$ and $\mu_B = 22.65 \pm 0.06$. Given the uncertainties in this calculation, this shows that our overall results are stable and robust.

Accurate flat-fielding is paramount for reliable surface photometry of low surface brightness features. As mentioned previously, we used blank sky fields near our target objects to construct a master night sky flat. For each sky frame, we masked stars and background objects by running IRAF's *objmask* task twice – once to generate a basic mask, then again with the first mask applied to mask even fainter sources; both times we masked objects using a threshold of 4 σ above background and 5 *sigma* below (more details on the masking procedure can be found in Rudick et al. 2010a). We then calculated the median values in 32×32 pixel blocks, and binned the images using these median values in order to enhance any faint, extended contaminants that were missed by *objmask*, such as flares from stars off the edge of the chip, extended wings of stars, and internal reflections. These features we masked by hand, and images with obvious large-scale contamination (faint cirrus clouds, unusual electronic noise) were discarded. We median combined all of these masked sky images to create a preliminary sky flat, re-flattened the sky frames using this flat, and modeled and subtracted sky planes from each flattened image. We used these flattened, sky-subtracted images to create a new flat, which we then used as a basis to repeat the process. The flat-field converged after five such iterations, resulting in the final generation master sky flat.

To test for systematics in the flat-fielding, we used this process to construct three types of master flats: master flats by object (all objects imaged during the course of this project, including targets other than the M96 Group), master flats by observing run, and a master flat made from all skies taken over the course of an observing season. We divided all pairs of these master flats to check for systematic differences, and we determined that there only existed a low-level (0.2%) residual plane that varied from run to run. As such, we created flat fields for each observing run by using the master flat generated from all sky images, corrected for each run's residual plane. In this way, our final B flat combined 98 total sky images, and our final V flat combined 123 total sky images. We note that the consistency of the flats (including even those taken nearer to Mars than the M96 Group) shows that scattered light from Mars was not a problem in constructing the flat field.

Bright stars can also introduce extended halos of light due to reflections between the CCD, dewar window, and filter; we modeled and removed these using the process described in Slater et al. (2009), for which we give a brief summary here.

[6] IRAF is distributed by the National Optical Astronomy Observatory, which is operated by the Association of Universities for Research in Astronomy (AURA) under cooperative agreement with the National Science Foundation.

[7] data located at: http://www.spaceweather.ca/solarflux/sx-eng.php

Table 1
Properties of streamlike features

Region	Dimens (′)	Dimens (kpc)	μ_B	μ_V	M_B	M_V	B-V (Range)	$\mu_{B,lim}$	$\mu_{V,lim}$	$10^6 L_{\odot,B}$
A	1.3×9.4	4×30	29.3±0.3	28.8±0.3	-12.2	-12.6	0.45(-0.14 – 1.04)	30.9	30.5	12
B	1.1×5.2	3.5×17	29.2±0.2	28.6±0.3	-11.6	-12.1	0.56(-0.08 – 1.15)	30.9	29.9	7
C North	1.1×9.6	3.5×31	29.8±1.0	29.6±0.8	-11.7	-11.9	0.21(-1.60 – 2.55)	30.1	29.7	7
C South	1.3×7.0	6×22	29.9±1.0	29.1±0.8	-11.4	-12.1	0.77(-1.04 – 3.11)	30.1	29.7	6
C Total	1.2×60.1	3.5×200	29.9±1.0	29.4±0.8	-13.9	-14.4	0.49(-1.32 – 2.83)	30.1	29.7	56[a]

Note. — *a*: Assumes a continuous structure from C North to C South: see text.

To generate visible reflections, we took long (1200 s and 900 s in B and M, respectively) exposures of zeroth magnitude stars (Procyon in B and Regulus in M). We modeled these reflections as annuli of constant brightnesses scaled by the total brightness of the parent star. We also measured and modeled the offset of each reflection from the parent star as a function of the star's position on the CCD. Lastly, we modeled the star's point spread function out to where the flux from the star drops to 0.3 ADU ($\mu_B \sim 31$). We then subtracted these models from each bright star in each image. Bright stars also produce visible off-axis reflections colloquially known as "Schmidt Ghosts" (Yang et al. 2002); we masked these as well for stars brighter than $V = 10.5$. To obtain accurate photometry for the bright stars producing these various reflections, we used short exposures of our target fields; for the brightest stars we used magnitudes given in the Tycho II catalog (Høg et al. 2000), and in a few cases (for stars with $m_B \lesssim 8$) we had to manually adjust the magnitudes to achieve the best subtraction.

We then masked and median binned the images into 32×32 pixel blocks, hand-masked any scattered light pattern in each object frame in the same manner as the blank skies, as well as any persistent bright objects in each frame. We fitted a sky plane to each of these binned, masked images, and subtracted this sky off of the original images. Finally, we mosaiced all of the resulting images using IRAF's *Wregister* and *imcombine* tasks, scaling each image to a common zeropoint, and creating 9×9 pixel and 18×18 pixel masked and median binned images to help identify faint features and improve the per pixel statistics in the final mosaics[8]. The masking process used to generate these images typically only masks pixels brighter than $\mu_B \approx 27$ and $\mu_V \approx 26$, so that the faint, diffuse signals we are searching for remain visible.

3. LARGE SCALE DIFFUSE LIGHT

Figure 2 shows our final 18×18 pixel ($26'' \times 26''$, or 1.4×1.4 kpc^2) binned B and V mosaics. This binning choice is simply to enhance the clarity of the features of interest; all analyses of the images used either the unbinned image or a 9×9 binned image. A schematic is provided in Figure 4 to guide the eye.

The first thing to note in these images is that we see no large-scale diffuse stellar counterpart to the HI ring. While there is a band of diffuse light running across the image in the B mosaic, the same feature does not appear in the V mosaic, which shows a different pattern of diffuse light elsewhere in the image. Permanent features such as starlight or foreground Galactic dust lanes ('cirrus') should remain fixed in position and morphology from image to image, whereas scattered light patterns will change with respect to the position of the source. As noted in Section 2.1, Mars was less than 3° from our fields in Spring of 2012, when we observed in the B filter, and hence may have contributed to the scattered light in the final B mosaic. It is less clear where scattered light may have originated in the V mosaic, with the brightest nearby source (Regulus) being ∼ 9° to the west. Regardless, as the only diffuse signal we see appears to be scattered light, we find no evidence of actual diffuse starlight in the Leo HI ring. We place upper limits of $\mu_B < 30.1$ and $\mu_V < 29.5$ on the surface brightness of any such component, as these are the average surface brightnesses of the scattered light signals found in the southern portion of the Ring (where the bulk of the HI mass is found). We note that this is consistent with an estimate by Castro-Rodríguez et al. (2003) of $\mu_B < 32.8$ based on the apparent lack of planetary nebulae associated with the cloud.

Despite this lack of large scale diffuse light in the Ring, we do find three smaller features, which are labeled in Figures 2 and 3 and shown schematically in Figure 4: a streamlike object north of NGC 3384 (A), a shorter streamlike object northeast of M95 (B), and a nearly vertical streamlike object west of NGC 3384 and the background galaxy NGC 3389 (C, most clearly visible in the V band image). While these features are consistent in morphology and position in both mosaics, they are extremely faint, so to further test their consistency we created three sets of new B and V mosaics using randomly selected half-samples of the object frames used to build the final mosaics in each band. All three objects persisted even in these half-split mosaics. We note also that all three features are visible in a preliminary data set taken in 2010 in the M band, so the three features appear to be robust. Other structures are visible in Figures 2 and 3, such as a V-shaped structure on the images' west sides, but these were not consistent in morphology amongst all half-splits and so were not considered for analysis.

Finally, as scattered light from galactic dust (the so-called "Galactic cirrus") can often show similar diffuse morphology, we cross-checked our mosaics against the IRIS 100 μm map (Miville-Deschênes & Lagache 2005) for the region. As cool dust emits thermally in the far-infrared, any contamination from galactic cirrus should show corresponding emission in the 100 μm map. However, this map shows that the M96 Group lies in a region with relatively little such foreground pollution, and shows no spatially corresponding linear structures. The Planck all-sky thermal dust emission map (Planck Collaboration 2013), though lower resolution, confirms this as well. This lack of detection in the far infrared makes it unlikely that these features are merely foreground dust, and thus are likely to be tidal structures located within the M96 Group.

[8] For the sake of efficiency, for the remainder of the paper we will refer to the process of masking and calculating the median in blocks as simply 'binning'. As such, references to e.g. the '9×9 binned image' refer to the image that has been masked and then median-binned into 9×9 pixel blocks.

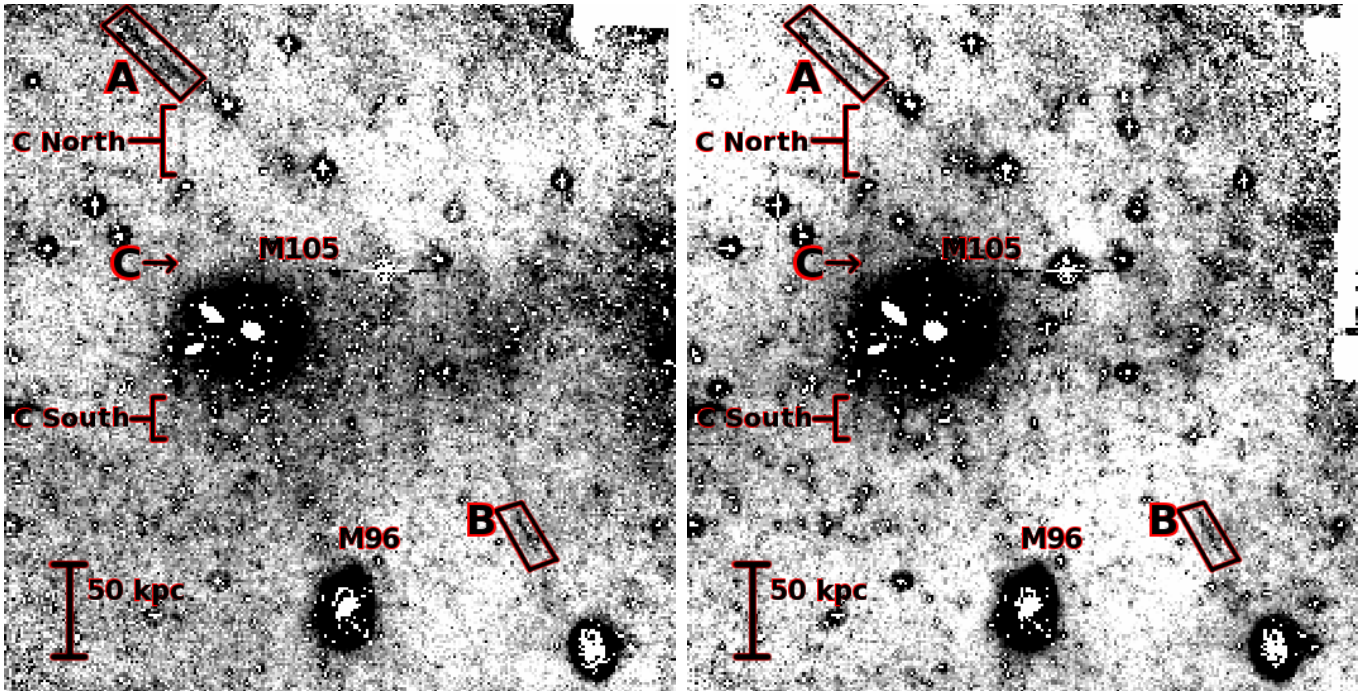

Figure 2. Our final B mosaic (left) and V mosaic (right), with pixels binned 18×18 to improve the clarity of the features of interest. The three regions discussed in the text are labeled A, B, and C; due to the faintness of region C, its general position is indicated only by an arrow. C North and C South indicate where the photometry for the feature was performed, with the brackets showing the extent of the regions sampled. M105 and M96 are labeled for reference. In both images, dimensions are $1.9° \times 1.9°$ (360×360 kpc^2), and north is up and east is to the left. Boxes are for illustration purposes only. Contrast is such that pixels saturate below $\mu \sim 28.5$. Images are masked at high ($\mu \lesssim 24$) surface brightness.

In addition to the linear streams, we also detect diffuse starlight around the galaxy KK96 (located southwest of NGC 3384). This galaxy, classified as a low surface brightness dwarf spheroidal (dSph) by Karachentseva & Karachentsev (1998) and Karachentsev et al. (2013), displays clear tidal tails toward the east and west in our images (clearly visible even in the unbinned images: see Figure 3), indicating a recent interaction. Due to a lack of distance constraints for this galaxy, its relation to the M96 Group is unclear. However, aside from the M96 Group, it appears to have no obvious nearby neighbors that it may have interacted with.

We can attempt to constrain KK96's location to some degree through its optical properties. The galaxy has an apparent magnitude of $V = 16.9$, including all light out to the Holmberg radius (0.6′; see Karachentsev et al. 2013) and excluding the faint tails. We also measure an effective surface brightness ($r_e = 0.3'$) of $\mu_{e,V} = 25.8$ and central surface brightness of $\mu_V \approx 23$. If placed at the distance of the M96 Group, the galaxy would have an absolute magnitude of $M_V = -13.3$, similar to the Fornax dwarf (van den Bergh 2008), and an effective radius of 960 pc, consistent with the empirical M_V–$\mu_{e,V}$ and M_V–r_e relations for Sph type galaxies from (Kormendy & Bender 2012). If the system is significantly closer, for example within the Local Group at 1 Mpc, the galaxy would be underluminous by ≈ two magnitudes for its surface brightness, given the Kormendy & Bender relation. However, given the scatter in the dSph scaling relationships, the system is also consistent with being a member of the background Leo II galaxy group (at a distance of ∼20 Mpc; see Stierwalt et al. 2009). So while it is *plausible* that the system is being tidally stripped by its interactions within the M96 Group, without proper distance constraints, it is difficult to state this unequivocally.

The properties of the three linear features labeled A, B, and C, including local limiting surface brightnesses and color constraints, are summarized in Table 1. Absolute magnitudes and luminosities are calculated assuming a distance of 11 Mpc, and are similar to moderately-sized dwarf galaxies, although we point out that we see no actual dwarf galaxies associated with the features themselves. The wide range in the estimated colors is due to the low light levels of the three features; a large uncertainty in surface brightnesses corresponds to a much larger uncertainty in associated color. As such, we are unable to make any definitive statements regarding the stellar populations in these features.

We perform photometry on the three features using apertures that include all of their visible light, subtracting off a locally-measured background level, which produces more accurate photometric results (see Rudick et al. 2010a). We measure the background flux by averaging the counts in several (4 to 6, depending on the proximity of obvious contaminating background or foreground sources) comparably sized blank sky regions surrounding the signal region, and use the dispersion in the median values of the blank regions as our measure of background uncertainty (for examples, see Rudick et al. 2010a; Mihos et al. 2013a). This dispersion in ADU is then converted to a local limiting surface brightness.

To determine the likelihood that these features are in any way associated with the HI ring, we overlay HI contours from Schneider (1989) and Michel-Dansac et al. (2010) on our binned V mosaic for comparison. This is shown in Figure 3. Interestingly, the northernmost stream, labeled A, roughly follows the northwest arc of the HI ring. The feature may extend farther to the southwest, but is obscured by a foreground star. Assuming an area of $1.3' \times 9.4'$ (4×30 kpc^2),[9] the to-

[9] It should be noted that the boxes depicted in Figures 2 and 3 do not correspond to the dimensions given here, and are merely for illustrative purposes.

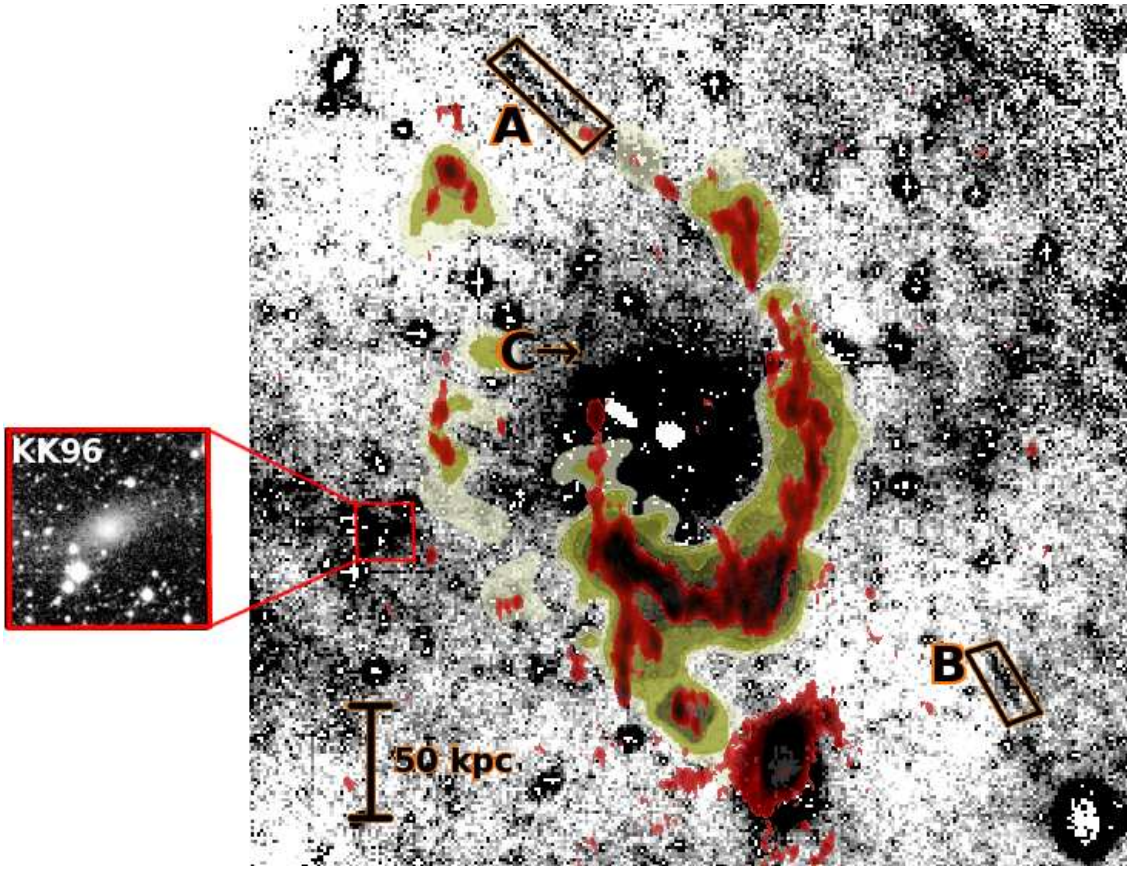

Figure 3. Our final V mosaic, binned 18 × 18 as in Figure 2, with HI contours from Schneider (1989) and Michel-Dansac et al. (2010) overlaid in yellow and red, respectively. The three regions from Figure 2 are labeled for reference, as is the dwarf galaxy KK96 (see text). The inset image is the unbinned image of KK96, zoomed in for clarity, to show the tidal tails more clearly. Again, the image is 1.9° × 1.9° (360 × 360 kpc^2) with north up and east to the left, and boxes are for illustration purposes only.

tal flux from the feature yields an absolute B magnitude of $M_B = -12.2$, for a surface brightness of $\mu_B = 29.3 \pm 0.3$ mag arcsec^{-2}. This corresponds to a luminosity of roughly $1.2 \times 10^7 L_{\odot,B}$.

Stream B lies near M95, well away from the HI ring. Given this apparent separation, it may not be associated with the Ring complex at all. Its linear morphology and lack of any central nucleus does imply that it has been tidally disrupted, and so it may be an object similar to KK96 but lower in mass, possibly a satellite of M95 given its apparent proximity to the galaxy. Assuming an area of $1.1' \times 5.2'$ (3.5×17 kpc^2), we find $M_B = -11.6$ and $\mu_B = 29.2 \pm 0.2$, for a total luminosity of $7 \times 10^6 L_{\odot,B}$.

Finally, Stream C appears to be one long linear feature, extending from just below feature A southward almost 10′ before disappearing below NGC 3389. This feature is unlikely to be an instrumental artifact, as it does not align along the rows or columns of the CCD. It lies near a similar vertical linear feature in the HI, although it is displaced to the east and tilted in position angle by ∼ 1°. The northernmost cloud of this HI feature appears associated with NGC 3384 in both proximity and velocity, however the association of the two small clouds just to the south is more ambiguous (Oosterloo et al. 2010). For the northern end of the optical feature (labeled C North), sampling from an area of $1.1' \times 9.6'$ (3.5×31 kpc^2), we find $M_B = -11.7$ and $\mu_B = 29.8 \pm 1.0$. For the southern end (labeled C South), an area of $1.3' \times 7.0'$ (4×22 kpc^2) yields $M_B = -11.4$ and $\mu_B = 29.9 \pm 1.0$. Uncertainties are calculated under the assumption that the north and south ends are pieces of one unique structure; as such, dispersion in the "local" background is calculated using apertures in blank regions around both the north and south ends. This is a conservative approach; if the north and south ends are taken individually, the local dispersions are much lower. For the whole structure, if we assume an average surface brightness of $\mu_B = 29.9$, and a constant shape from the southern tip to the northern tip (a total projected length of ∼ 200 kpc), we calculate a total absolute magnitude of $M_B = -13.9$, which corresponds to a luminosity of $5.6 \times 10^7 L_{\odot,B}$.

The proximity of features A and C to similar-looking features in the HI is intriguing. Similar streams of diffuse starlight have been found in the Virgo cluster near M87, which are thought to be collisional in origin (Mihos et al. 2005), so this may well be the case for these features as well – these may be the remnants of small galaxies tidally disrupted by the group potential. In this collisional picture, however, feature B stands out as unusual given its large distance from the central galaxy, M105. Recent observations from the ALFALFA survey (Stierwalt et al. 2009) show no HI detection in its vicinity, making its association with the M96 Group much more ambiguous.

Given the rough spatial correspondence between A and C and the HI, it is useful to compare these results with some of the proposed models for the formation of the HI ring. The collision model given by Michel-Dansac et al. (2010), for example, predicts a diffuse halo of starlight to have been generated at a surface brightness $\gtrsim$29 mag arcsec^{-2}. In terms of a diffuse component, again, we find nothing up to $\mu_B = 30.1$ and

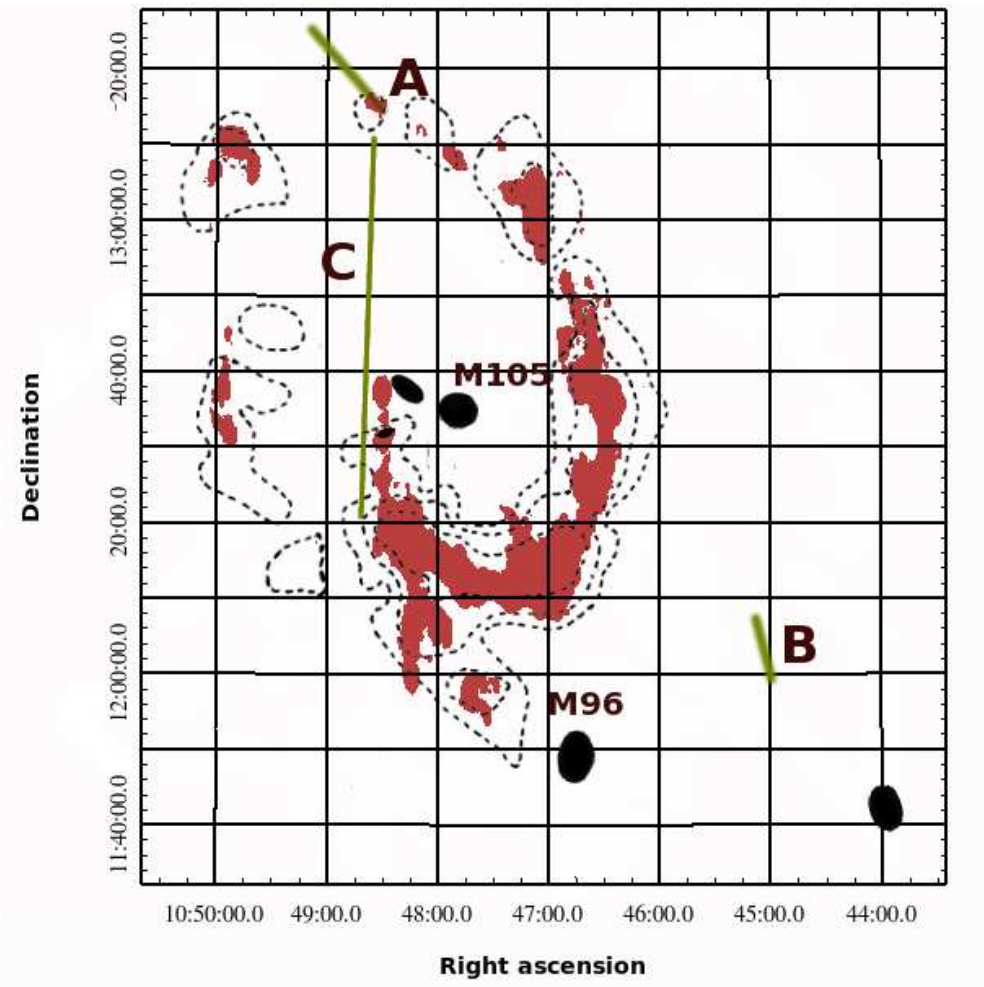

Figure 4. Schematic of the three features in relation to the group galaxies and the HI ring, for clarity.

μ_V = 29.5; if there is such a diffuse halo component, it must exist at levels even dimmer than this. The model by Bekki et al. (2005), on the other hand, seems to predict no stellar component whatsoever, although it does require the presence of a low surface brightness (LSB) disk galaxy. In their simulation, this galaxy's gaseous disk is stripped to smaller radii, with the stellar component left basically intact. No such small isolated gaseous disk has been found in the HI surveys that have been done on this group (Schneider et al. 1989; Stierwalt et al. 2009), and we discover no heretofore unseen LSB disk in our imaging, despite that the simulation by Bekki et al. (2005) predicts that such a remnant should remain within 200 kpc (1.5°) of the group center (see their Figure 1).

Regarding the streamlike features themselves, given their faintness, we can only make general guesses at their physical nature. For example, we might assume, given the luminosities we calculate, that these features are tidally-stripped dwarf galaxies. Dwarf galaxies are low mass, and hence typically have low velocity dispersions (of order 10 km/s; see e.g. Mateo 1998, and references therein). After disruption, the system is no longer gravitionally bound, and so the internal random motions should serve to widen the remnant stream over time. Assuming a characteristic velocity dispersion of 10 km/s, and given their current widths of roughly 5 kpc, this would imply an interaction timescale of order 500 Myr, shorter than the 1.2 Gyr predicted by Michel-Dansac et al. (2010), and far shorter than the 4 to 6.5 Gyr proposed by Bekki et al. (2005). However, without kinematic data, it is hard to place robust constraints on formation scenarios for these features.

Finally, the only previously known stellar counterparts to the Ring were the three star-forming clumps discovered by Thilker et al. (2009) and later verified by Michel-Dansac et al. (2010). We corroborate this discovery in our imaging as well in the form of three unresolved patches of light coincident with – and with morphologies very similar to – the FUV and NUV emission, and again with blue colors ($B - V$ between ∼-0.1 and ∼0.4, see Figure 5). Thilker et al. (2009) and Michel-Dansac et al. (2010) came to opposite conclusions regarding the nature of this star formation, the former finding a best-fit model to their UV colors with a low metallicity, several hundred Myr burst, and the latter finding that their SED was fit best by a pre-enriched, 5 Myr instantaneous burst akin to the star-forming region NGC 5291N (within the galaxy NGC 5291). While we cannot constrain either model, it is clear from our data that these star-forming regions are isolated events within the Ring, rather than part of any extended tidal stream of old stars, and thus represent a pure sample of stars that have formed directly out of it. This makes them an ideal target for future observations in the effort to measure the metallicity of the Ring directly. In addition, as these regions are several kpc across, they may represent dwarf galaxies that are in an early stage of formation; obtaining a CMD of these stars would thus provide further important constraints on the origin of the Leo Ring, and thus further constraints on forma-

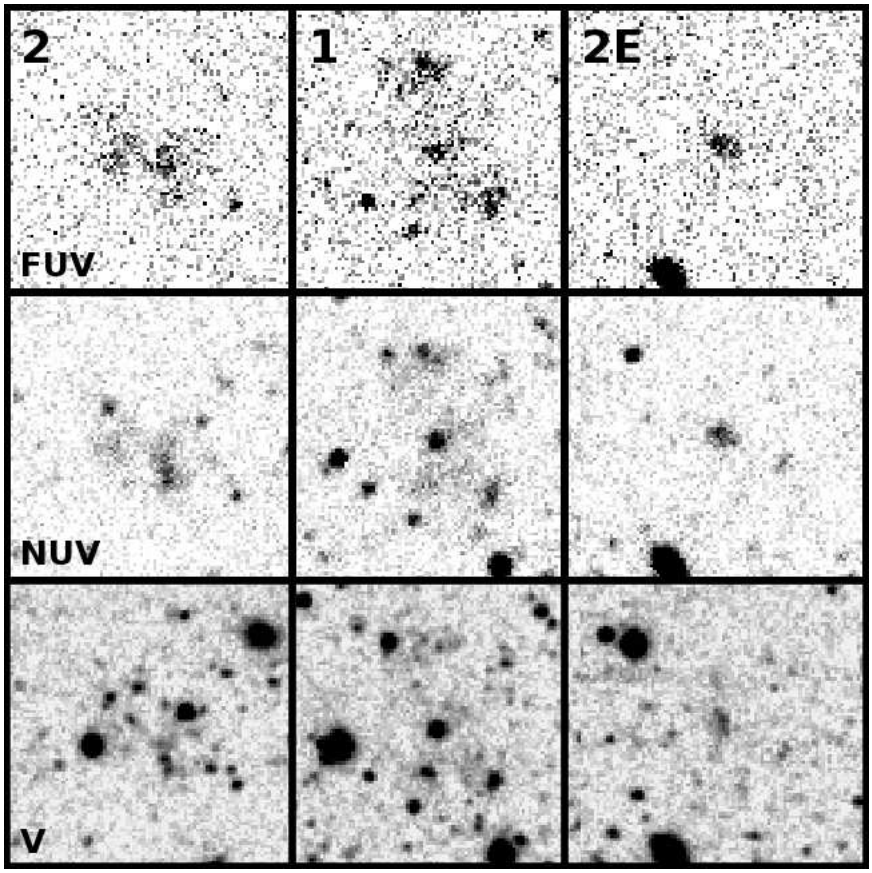

Figure 5. Comparison between GALEX FUV (top row), NUV (middle row), and our optical data (V band, bottom row) for the three dense HI regions discussed in (Thilker et al. 2009) and (Michel-Dansac et al. 2010). The region labels 2, 1, and 2E refer to the nomenclature used by Thilker et al. (2009). Each box is approximately 2.5′ on a side (8 kpc). Measured optical colors of the diffuse emission (not including point sources) in these regions are as follows. Region 2: $B - V = 0.2 \pm 0.2$; Region 1: $B - V = 0.0 \pm 0.1$; Region 2E: $B - V = 0.1 \pm 0.2$. Uncertainties are due mainly to the small sizes of the regions.

tion mechanisms of dwarf galaxies (e.g. formation from tidal encounters or out of primordial HI clouds; Lynden-Bell 1976; Barnes & Hernquist 1992; Metz & Kroupa 2007; Pawlowski et al. 2012).

4. INDIVIDUAL GALAXIES

The streamlike features discussed in the previous section, while intriguing, remain ambiguous in origin and nature due to poorly constrained colors and lack of distance and velocity data. However, if the collisional origin hypothesis is correct, evidence of the past encounter that produced the features may be found in the group's galaxies themselves. We now turn to the individual galaxies, searching for accretion signatures and quantifying the structure and stellar populations in their outer regions.

Here we present photometric profiles of the group's four bright galaxies: M105, NGC 3384, M96, and M95. Each annulus from which the azimuthally averaged photometric values are derived takes into account changing ellipticity and position angle, measured as a function of radius using IRAF's *ellipse* function (for details, see Jedrzejewski 1987). Also for each galaxy, we measure profiles along six constant angular-width wedges, using a constant position angle and ellipticity derived from the last isophote fit by *ellipse*, to look for asymmetries in each galaxy that would otherwise be washed out by azimuthal averaging. All magnitudes and colors are corrected for foreground Galactic extinction using the values of $A_V = 0.067$ and $E(B - V) = 0.02$ from Schlafly & Finkbeiner (2011).

4.1. *M105*

M105 (NGC 3379) is a classic elliptical galaxy, most famous for being a keystone of the de Vaucouleurs $r^{1/4}$ photometric profile (de Vaucouleurs & Capaccioli 1979). Observations in HI and CO have revealed a dearth of atomic and molecular gas (Bregman et al. 1992; Sofue & Wakamatsu 1993; Oosterloo et al. 2010), although there does exist a very small ($\sim 150\ M_\odot$) dusty disk in the inner 13″ (Pastoriza et al. 2000). The kinematics of the galaxy's center show some peculiarities, leading to speculation about whether it is actually a face-on triaxial S0 galaxy (Statler & Smecker-Hane 1999), although kinematics gleaned from planetary nebulae show little evidence of rotation out to 330″ (Ciardullo et al. 1993; Douglas et al. 2007). Schweizer & Seitzer (1992) analyzed the galaxy for evidence of recent interaction and found none. In total, aside from the innermost regions, the galaxy appears to be in a very relaxed, pressure-dominated state.

Figure 6 shows our photometry for this galaxy. It can be clearly seen that the $r^{1/4}$ model remains a good fit out to the extent of our data ($\sim 850''$, or 50 kpc), without significant variations within the uncertainty. The $B - V$ color profile shows a slope of $\Delta(B-V)/\Delta(\log r) = -0.04$ mag dex^{-1} out to $r^{1/4} \approx 4$, or 13.5 kpc (in modest agreement with Goudfrooij et al. 1994). Beyond $r^{1/4} \gtrsim 4.2$ (310″), the level of uncertainty in the colors as indicated by the large dispersion amongst the different angular profiles makes determination of colors impossible. Out to the 25^{th} magnitude isophote, we measure an integrated color (before reddening correction) of $B-V = 0.96$,

in perfect agreement with the Third Reference Catalog (RC3 de Vaucouleurs et al. 1991) value of $(B-V)_T = 0.96$.

We see no non-axisymmetric structure in either the surface brightness or color profiles, so to investigate more thoroughly whether M105 shows any signs of interaction, we created an elliptical model of the galaxy using IRAF's *ellipse* and *bmodel* functions and subtracted this from our image. This is the same procedure outlined in Janowiecki et al. (2010), performed under the assumption that local density variations will show up as residuals after subtraction of a smooth profile. The results are shown in Figure 7.

The only readily apparent structure in the residual image appears near the center of the galaxy, in the form of a pinwheel-like structure. Such residual artifacts are commonly seen (see, e.g., Janowiecki et al. 2010), and are a sign of slight non-ellipticity in the galaxy isophotes rather than any truly distinct structural component. Another much fainter source appears, marginally detected, a few arcminutes to the northwest of the galaxy's center, which may be an extremely faint shell ($\mu_B \approx 29.3$, measured from the subtracted image to isolate the feature). We have verified that the isophotal model itself has no artifacts that would imprint such features, and an independent application of the technique on the V band image also reveals these structures. Other than these weak features, however, the galaxy appears to be well-modeled by smooth elliptical isophotes with no sign of recent accretion. Consistent with previous studies, then, M105 appears remarkable in just how unremarkable it is.

Our data implies that if any unusual formation signatures are left to be found in M105, they must lie in the galaxy's stellar populations. Indeed, Harris et al. (2007) studied the discrete stellar populations in M105's outer halo at a radius of $\sim 540''$ ($r^{1/4} = 4.8$) and found evidence for a substantial population of low metallicity stars. If the outer halo is significantly more metal poor than the inner regions, this should result in systematically bluer isophotes, modulo differences in mean stellar age between the halo and inner galaxy. If anything, our data suggest the metallicity gradient becomes more shallow, indicative of a redder stellar population in the halo, but at the extremely low surface brightness characteristic of the outer halo ($\mu_B > 28$), the uncertainty in our color measurements is extremely large and makes quantitative comparison difficult.

4.2. *NGC 3384*

NGC 3384 is a lenticular galaxy in close proximity (in projection) to M105. Like M105, it too is nearly devoid of gas (Sage & Welch 2006; Oosterloo et al. 2010) and dust (Tomita et al. 2000), and Busarello et al. (1996) found a fairly flat color profile at around $B-V \approx 0.9$ out to $40''$, typical for S0 galaxies (Li et al. 2011). The galaxy also contains several "faint fuzzies" (Larsen et al 2001), globular cluster-like objects with large half-light radii (R_{eff} = 7 - 15 pc, versus 2 to 3 pc in normal GCs), which Burkert et al. (2005) hypothesize may have originated in a low impact parameter galaxy collision. Previous work has also shown the galaxy to be host to a number of other notable peculiarities, including strong isophote twists (Barbon et al. 1976; Busarello et al. 1996), a pseudobulge or double-bar (Pinkney et al. 2003; Erwin 2004; Meusinger et al. 2007), and outer boxy isophotes (Busarello et al. 1996). NGC 3384 thus appears much less well-settled than its neighbor M105.

Figure 8 shows our profiles for this galaxy. It has a roughly exponential surface brightness profile out to $\sim 325''$; beyond this radius, the profile becomes flatter and may simply mark the transition into the local background. Asymmetry is seen near the center (within $40''$), resulting from the bulge/bar complex, and from $\sim 100''$- $150''$, where a hump appears in the azimuthally averaged profile. The color profiles appear mostly flat at $B-V = 0.88$ out to a radius of $\sim 200''$, after which they redden. This redward color gradient does not appear to be due to influence from the neighbor M105; at this radius, M105's surface brightness is $\mu_B = 28.5$, compared to NGC 3384's $\mu_B = 25.5$. The surface brightness profile appears to show a mild anti-truncation at this radius as well, although the strong deviations from an exponential profile in the rest of the disk make this difficult to quantify. We measure an integrated color (without extinction correction) of $B-V = 0.92$, in good agreement with the RC3 value of $(B-V)_T = 0.93$.

To further investigate NGC 3384's outer structure, as we did for M105, we subtracted a smooth model for NGC 3384 to search for residuals. This is also shown in Figure 7. Unlike with M105, however, we discover very clear residuals from the smooth profile in the form of two arcs northeast of the galaxy center, as well as a diffuse plume protruding out toward the southwest. Again, all of these features are seen when subtracting a model from the V image as well. The northeast arcs appear much less sharp than arcs often seen in elliptical galaxies (e.g. Malin & Carter 1983), which are thought to be formed via minor mergers (Hernquist & Quinn 1987). The binned image reveals another faint structure toward the south, as well as a possible bridge connecting the innermost arc to the southwest plume, which would imply more of a ring or disk shape.

The inner arc appears at a radius of $\sim 120''$, and fades at $\sim 165''$. It has a surface brightness of $\mu_B \approx 27.5$ with the underlying disk subtracted. In this region, the northeast (blue) profile from Figure 8 is brightest, followed by the northwest (green), with the southeast (red and purple) apparently following a more regular exponential disk profile. This behavior appears to reflect the location of the arc, though it is interesting to note that we see no color deviations in this region. The southwestern plume appears at roughly the same radius; however, due to the presence of M105, we can say little about the structure of the disk in its viscinity. The plume has an average surface brightness of $\mu_B \approx 27.8$ and a much less regular morphology, making its nature more ambiguous. The outermost arc appears from a radius of $\sim 200''$ to $\sim 275''$, the location of the red color gradient (and possible anti-truncation). This arc is only slightly fainter than the inner arc: $\mu_B \approx 27.8$. These surface brightnesses correspond to absolute magnitudes of $M_B \sim -11.7$ and $M_B \sim -12.1$ for the inner and outer arcs, respectively, and $M_B \sim -12.2$ for the southwestern plume, which implies progenitors with the luminosities of a dwarf galaxy (e.g. Mateo 1998).

A 'faint extended luminous arc' in this galaxy, so described by Busarello et al. (1996), was photographed by David Malin in 1984 and appears to correspond spatially to this outer arc (Malin 1984, the photograph is shown in Busarello et al. 1996). As such, we would suggest based on our imaging that the arc discovered by Malin is actually part of a system of accretion features in the galaxy. This total system (inner arc, outer arc, and southwestern plume) has a combined luminosity of $\sim 3\times10^7 L_\odot$, again indicative of a fairly low stellar mass system.

At first glance, the surface brightness profile shown in Figure 8 is suggestive of an exponential disk with one or more breaks. However, the presence of the northwest arcs influ-

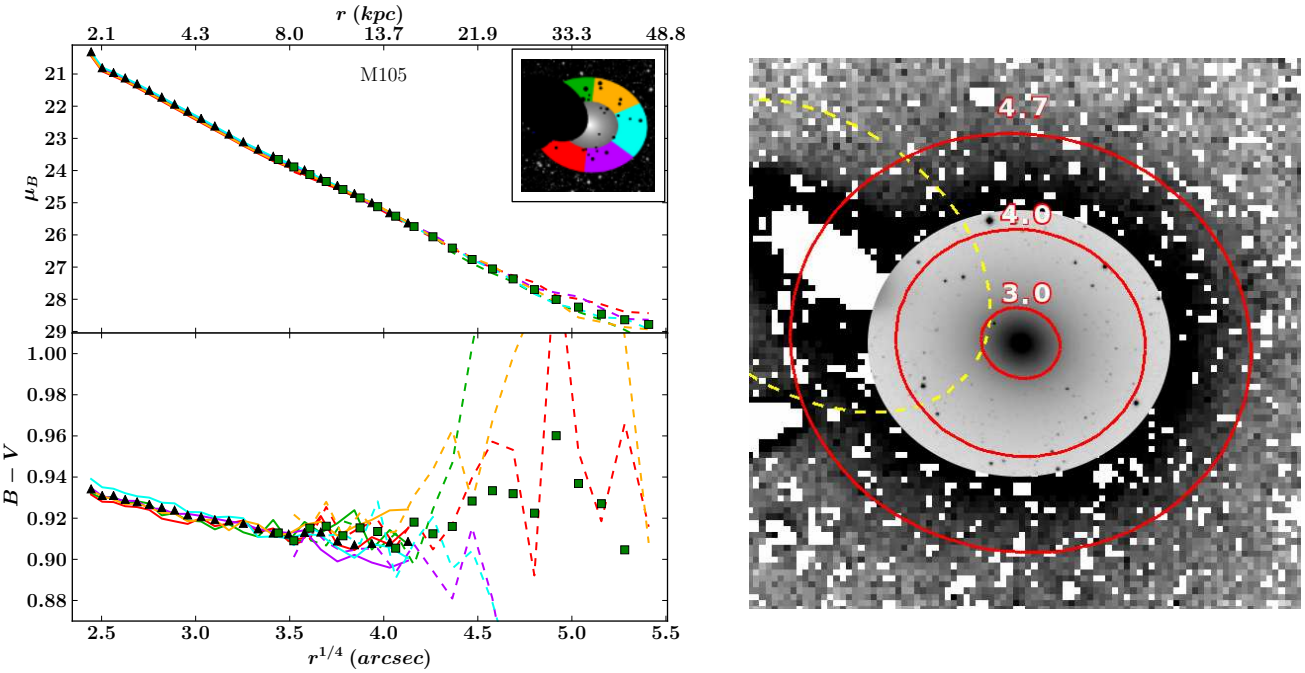

Figure 6. Left: B band surface brightness and $B-V$ color profiles for M105. The colored lines show the profiles of equal-angle cuts across the galaxy, which are shown schematically in the upper right of the figure (solid black regions indicate masking). Solid lines indicate values derived from the unbinned mosaic, and dashed lines indicate use of the 9×9 binned mosaic. Likewise, black triangles are azimuthally averaged values in the unbinned image, and green squares are azimuthally averaged values in the 9×9 binned image. The abscissa shows length of the semi-major axis in units of arcsec$^{1/4}$. Physical scale is given along the top axis assuming a distance of 11 Mpc. **Right:** diagram of the galaxy with three labeled ellipses, for reference. The values shown are in units of $r^{1/4}$ in arcseconds. The unbinned image is shown inside of $r^{1/4} \approx 4.1$, and the 9×9 binned image is shown outside of this radius. The yellow dotted ellipse indicates where NGC 3384 was masked out.

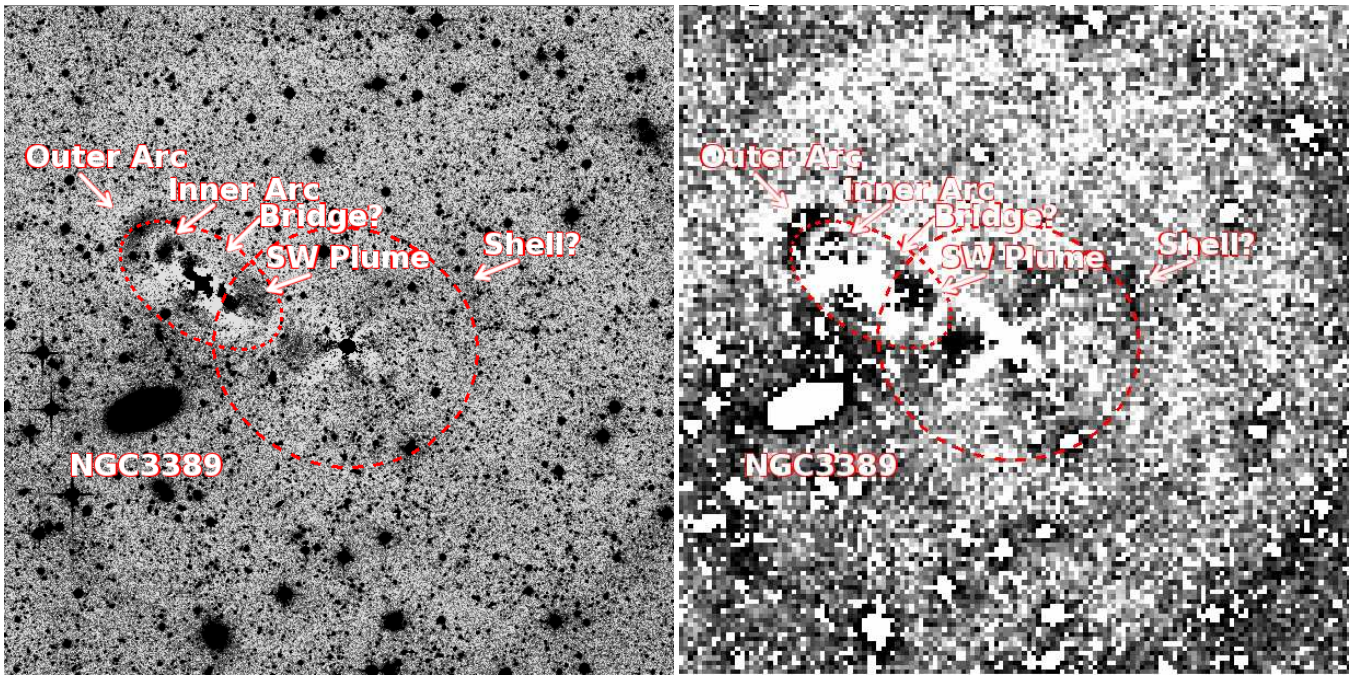

Figure 7. Left: unbinned B image of NGC 3384 and M105 after subtracting out models of both galaxies. Red dotted ellipses correspond to the $B = 26.5$ magnitude isophotes for both galaxies. North is up and east is to the left. **Right:** as left, but median binned into 9×9 pixel bins. We note that independent model subtractions on the V image show similar results.

ences the major axis profile, resulting in the hump at 100″. Instead, the profile along the southwest wedge (shown by the red curve), away from the arcs, more accurately follows the true underlying disk structure: a pure exponential out to at least 16 kpc, or approximately 8 scale lengths. Only at larger radii do we see any suggestion of a break in the profile, in the form of a possible anti-truncation of the disk in its outermost regions.

NGC 3384 thus provides an interesting contrast to the extremely well-settled M105. We see that the galaxy's unusual features are not constrained to the innermost regions – boxy isophotes exist as far out as 16 kpc, and the two arcs are strong evidence of disturbance. In some ways, this galaxy is similar to the face-on S0 Arp 227, discussed in Schombert & Wallin (1987). That galaxy showed similar shells with much less sharp morphology to the more standard shells often seen in elliptical galaxies, and with colors that deviated little if at all from the integrated color of the parent galaxy. Schombert & Wallin (1987) explained those features as possibly arising due to an accreted and subsequently evolved hot component from a neighboring massive galaxy (in that case, NGC 470). In NGC 3384's case, two obvious candidates for such an interaction would be M105 and M96, however, as shown in the previous section, M105 appears to show little sign of any dynamical disturbance in its recent past. At roughly 300″, NGC 3384's color is red enough ($B - V \approx 1$) to suggest an old halo population. The surface brightness profile begins to flatten here as well, as would be expected if an extended halo began to dominate the profile (Martín-Navarro et al. 2014). However, as previously mentioned, it is equally plausible within our uncertainty at these levels that we are simply seeing the contaminating influence of the scattered light in the image.

4.3. *M96*

M96 (NGC 3368) is one of two massive late-type galaxies in the group. The galaxy has long been known to have a faint outer ring or set of spiral arms originating at roughly 90″ (e.g. Schanberg 1973), which we clearly resolve as part of an outer disk with a position angle offset by more than 20° from the high surface brightness inner disk. These outer spiral arms primarily have long made it (along with NGC 3384) a favored candidate in the proposed collisional origin of the HI ring (Rood & Williams 1984; Michel-Dansac et al. 2010), as this level of asymmetry is difficult to produce via secular evolution processes. The galaxy's connection to the Ring was apparent from the Ring's initial discovery by Schneider et al. (1983) onward, with Schneider (1989) noting that, since most of its HI content exists in its outer disk, M96 may actually be accreting matter from the Ring.

Figure 9 shows our surface brightness and color profiles for M96. The galaxy shows a clear dip in its surface brightness profile between 85″ and 200″ (this 'dip' is what has been previously described as a Type II OLR, or Outer Lindblad Resonance, 'break' by Erwin et al. 2008). This appears to reflect a gap between the inner and outer disks. It is interesting to note that along the southeast and northwest profiles (the purple and green wedges, respectively), we do not see the dip, and in fact these profiles appear to have the same smooth exponential behavior as the outer disk, implying one continuous structure rather than, for example, an inner disk embedded in an offset outer ring. The color profiles show an asymmetry in this 'dip' region as well, bluer in the northeast than the southwest just outside of the inner disk. Another such asymmetric dip appears around 200″; these are most likely caused by HII regions in the northern arm, which are not visible in the much fainter southern arm. Beyond this radius, the color profile appears flat with some evidence of a continued northeast/southwest asymmetry even at extended radii, and the exponential surface brightness profile continues unimpeded to the extent of our measurements. Beyond 10 kpc, there is no evidence for a disk break in the outer disk, which shows a smooth exponential profile out to 25 kpc (7.5 scale lengths, as measured using the profile beyond 200″). Again, the integrated (uncorrected) color of $B - V = 0.85$ that we measure is in good agreement with the RC3 color of $(B - V)_T = 0.86$.

Most (> 60%) disk galaxies show breaks or truncations in their surface brightness profiles (Pohlen & Trujillo 2006), and while the inner disk of the galaxy does show a break, the lack of a truncation in the outer disk (beyond 10 kpc) is interesting. If we assume, based on the arguments of Pohlen & Trujillo (2006) and Erwin et al. (2008), that truncated disks are the normal end-state for spiral galaxies, the lack of truncation might imply that M96's disk is still being built. For example, mergers or accretion processes have been used to explain anti-truncations (Type III disks, e.g., Penarrubia et al. 2006; Younger et al. 2007) via deposition of excess light at large radius; it may thus be that mild star-formation in the outer disk of M96 caused by accretion from the HI ring is maintaining an exponential profile out to very large radii. The northeast/southwest asymmetry in our color profiles may reflect this process: the northeast side, which shows bluer colors at ∼85″ and ∼200″, is the direction from which the HI appears to be accreting (Schneider 1989). That these colors are only mildly bluer ($B - V = 0.7$, compared to 0.8 in the remaining angular wedges) and spatially localized (little azimuthal mixing even at the innermost radius, 85″) would imply that such star formation, if occurring, would be rather weak and somewhat recent, as it has not had time to azimuthally mix. The HI bridge is also visible in more detailed HI observations from Stierwalt et al. (2009), which also indicates that M96's HI disk is highly extended and lopsided, making the accretion hypothesis quite plausible (Bournaud et al. 2005).

That said, the overall impression from the data is that M96's outer stellar disk appears morphologically very smooth. The isophotes appear very regular, with the centroid of the outermost isophotes drifting south only by ∼15″ (a change of only ∼2.5%). If M96's outer disk is currently being built by accretion of gas from the Ring, it is apparently doing so in a very smooth and ordered way, despite the one-sided nature of the accretion and the lopsidedness of the accreted gas. A more plausible scenario may be that the accreted gas is collecting in the outer spiral arms and forming stars in those regions: Schneider (1989) showed that most of the galaxy's HI content is located within a dense ring located at roughly ∼200″(see their Figure 3), the location of the outer spiral arms (see Figure 9). This scenario does not easily explain the single-exponential nature of the outer disk, however.

4.4. *M95*

M95 (NGC 3351) is a barred spiral galaxy hosting a well-studied, star-forming circumnuclear ring (e.g., Alloin & Nieto 1982; Colina et al. 1997; Elmegreen et al. 1997; Comerón et al. 2010), as well as a larger ring of HII regions encircling the bar. It is the most isolated member of the group, and appears mostly undisturbed but for the star forming activity in the inner disk.

Figure 10 shows our surface brightness and color profiles for this galaxy. The bar and ring clearly influence the pro-

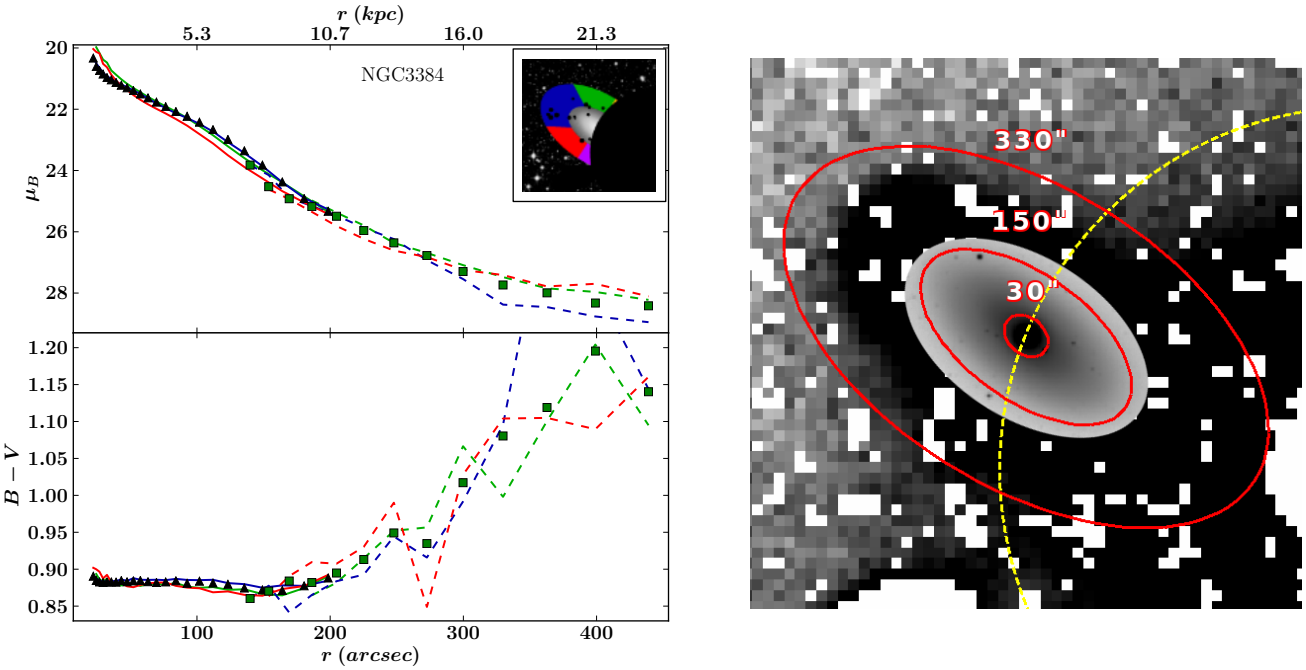

Figure 8. As Figure 6, but for NGC 3384. The units of the labeled ellipses in the right figure are now in arcseconds, and the yellow dotted circle represents where M105 was masked out. Only full wedges are plotted. We measure a scale length of 36.48″, or 1.9 kpc.

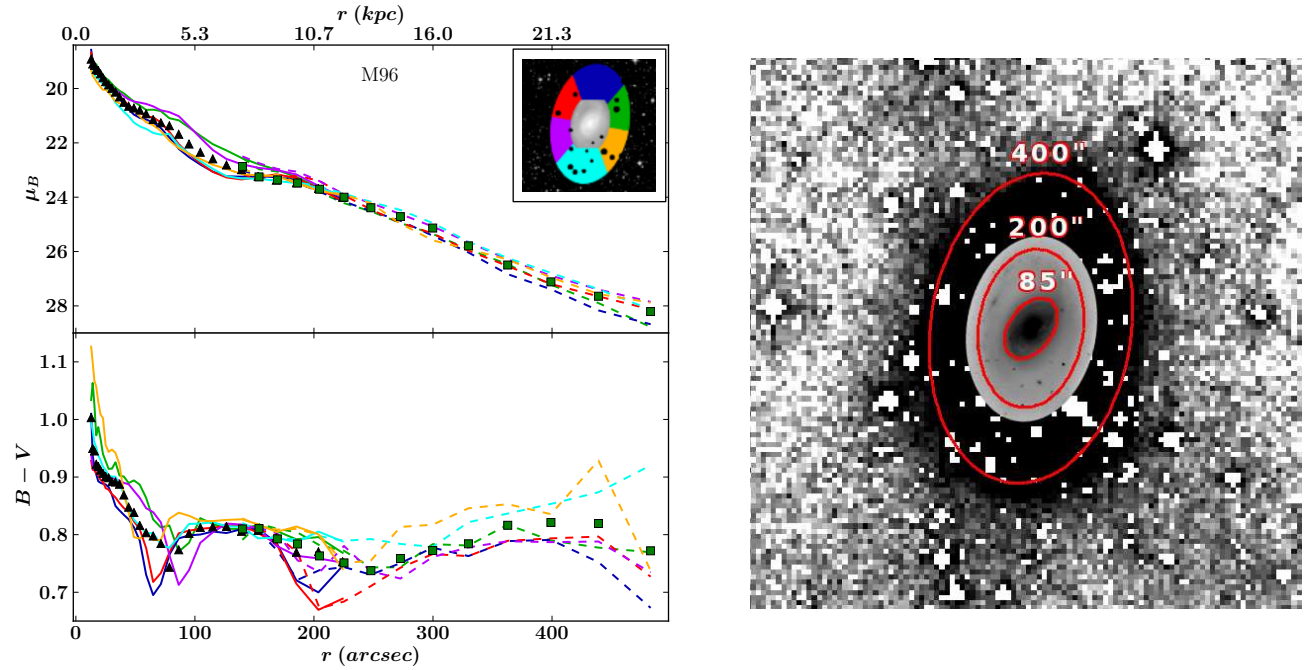

Figure 9. As Figure 6, but for M96. We measure a scale length of 61.04″, or 3.3 kpc (assuming a pure exponential profile).

files inside of 90″, with asymmetries resulting from spiral arms between 90″ and 130″ (again, the dip seen near 130″ has previously been classified as a Type II OLR break; Erwin et al. 2008). Beyond 130″, we see a smooth exponential disk (scale length 3.4 kpc) coupled with a mild blue color gradient, until a break and reversal in the gradient at ∼200″ (scale length 2.3 kpc). This broken exponential describes the disk morphology well to the extent of our data (400″ or 25 kpc). The outer isophotes of this galaxy appear quite regular, well-fit by smooth ellipses. No plumes or other asymmetries are visible even at extremely low surface brightness (≳29 mag arcsecond^{-2}). Once again, our measured integrated uncorrected color of $B - V = 0.78$ agrees well with the RC3 value of $(B - V)_T = 0.80$.

Given the presence of a distinct bar, a ring, and spiral arms in this galaxy, as well as the regularity of the outer isophotes (in both visible light and HI, e.g. Stierwalt et al. 2009), one possible explanation for the upturn in the color profile is an age effect due to outward radial migration of stars, driven by the non-axisymmetries in the inner disk (e.g., Roskar et al. 2008a,b). Such an effect has been observed in other galaxies; for example, consider the case of NGC 2403, in which Williams et al. (2013) discovered a flattening of the metallicity gradient beyond ∼12 kpc. Radial migration preferentially moves stars outward (Roskar et al. 2008a); the farther out a population of stars travels, the longer the travel time and hence the older the population must be (increasing age with increasing radius). A sample of uniform metallicity stars, like in NGC 2403, showing such a radial age gradient would tend to show a red color gradient as well. Thus a similar effect may be behind the behavior we see in M95's outer disk.

M95 thus appears to have no strong signatures of recent accretion in its outer disk. While its inner regions are tumultuous – Sérsic & Pastoriza (1967) classified it as a 'hotspot' galaxy – most of the star formation and other activity is well-described by resonances with, for example, the stellar bar (Devereux, Kenney, & Young 1992; Helfer et al. 2003). Given the galaxy's membership in the M96 Group, any interactions with other group members must have been extremely weak or have happened in the distant past, long enough ago that the outer disk has had time to recover. In §3, we suggested that Stream B (20′or 65 kpc away from M95, see Figure 3), rather than being associated with the Leo HI ring, may have resulted from the tidal disruption of a satellite galaxy interacting with M95. If so, the encounter appears to have made little impact on M95's outer disk.

5. DISCUSSION

5.1. *The origin of the Leo Ring*

In the context of the formation of the Leo Ring, arguably the most intruiging aspect of the M96 Group, the lack of either a diffuse stellar counterpart or strong interaction signatures in any of the group's four most massive galaxies is extremely puzzling. The imprint of strong interactions on the outskirts of galaxies (in the form of tidal features or distorted isophotes) should remain over the long dynamical timescales of the outer disks, yet we see no sign of such features in our imaging. This makes it hard to envision dynamical scenarios that invoke *recent* interactions to produce the Leo Ring. Even with our deep imaging, however, conclusive evidence favoring any particular formation scenario remains lacking. We describe below in more detail the connection between the observed structure of the Leo Group galaxies and the various formation scenarios for the Leo Ring.

5.1.1. *The case of M96 and NGC 3384: the collisional origin*

M96 and NGC 3384 (the two galaxies commonly proposed to have generated the Ring) demonstrate the difficulty in reconciling our results with collisional origin models for the Ring; while both galaxies show signs of disturbance (the arcs found in NGC 3384, and the position angle offset between the inner and outer disk of M96), it is unclear whether or not these could be the remnants of an interaction of the type proposed by Rood & Williams (1984) and Michel-Dansac et al. (2010). For instance, the type of morphology seen in M96 has occasionally been referred to as an 'oval distortion' and may actually be a result of secular evolution (Kormendy & Kennicutt 2004). The galaxy M94 (NGC 4736), for comparison, has a very similar morphology to M96, yet appears to have no nearby companions of significant mass (Trujillo et al. 2009).

However, the mildness of the interaction signatures we do find in the outer disks must constrain the timescale of any interaction model, as clearly any significant perturbation caused by an interaction has by now been erased. The simulation by Michel-Dansac et al. (2010) required 1.2 Gyr for the Ring to achieve its current size, which is roughly the orbital period of M96's extreme outer disk (based on the gas velocities of Schneider 1989). Yet M96's outer disk, the region most loosely bound and hence most easily perturbed, appears mostly smooth, with the exception of the slight southern skew shown in Figure 9. It is difficult to imagine how the galaxy's outer disk could settle so rapidly (in one orbital period) after such a strong encounter as envisioned by Michel-Dansac et al. (2010). To displace such a massive amount of gas into the Leo Ring while only leaving behind such mild signatures in M96's outer stellar disk would require a high interaction velocity (Spitzer & Baade 1951), while the group's low measured velocity dispersion (Pierce & Tully 1985; Stierwalt et al. 2009) would seem to imply a more tightly bound system. The timescale of 6.5 Gyr proposed by Bekki et al. (2005) may be more realistic in this regard, but again, the expected signature their model would leave behind (a gas-deprived, low surface brightness galaxy) does not appear to be present. The original scenario proposed by Rood & Williams (1984) appears even less likely due to its much shorter timescale (500 Myr).

Alternatively, rather than an encounter disturbing any pre-existing outer disk, it is conceivable that M96's outer disk was created by the encounter. The apparent accretion of HI onto M96 from the Ring is interesting in this context: recall the bifurcation in the color profile, with slightly bluer colors on the side nearest the Ring ($B - V = 0.7$) than on the farthest side ($B - V = 0.8$). While these colors are similar to the more quiescent, early type disk galaxies (Sa-Sab and S0a, respectively; see: Roberts & Haynes 1994), these are colors averaged over wedges; the northern spiral arm itself shows a number of large patches with colors of roughly $B - V = 0.4$, while the southern arm is nearly devoid of such regions. This is reflected in the GALEX FUV data as well (Martin et al. 2005), in which both arms are clearly visible at 200″, but the southern is visibly fainter than the northern. Measuring the FUV flux in the northern arm from the GALEX image and adopting the conversion to star formation rate given by Kennicutt (1998), we find a total star formation rate of 0.002 $M_\odot$ yr^{-1}over an area of roughly 45 kpc^2, whereas in the southern arm we find only 5×10^{-4} $M_\odot$ yr^{-1} over an area of 20 kpc^2. This thus implies star formation surface densities of 4×10^{-5} $M_\odot$ yr^{-1} kpc^{-2} in

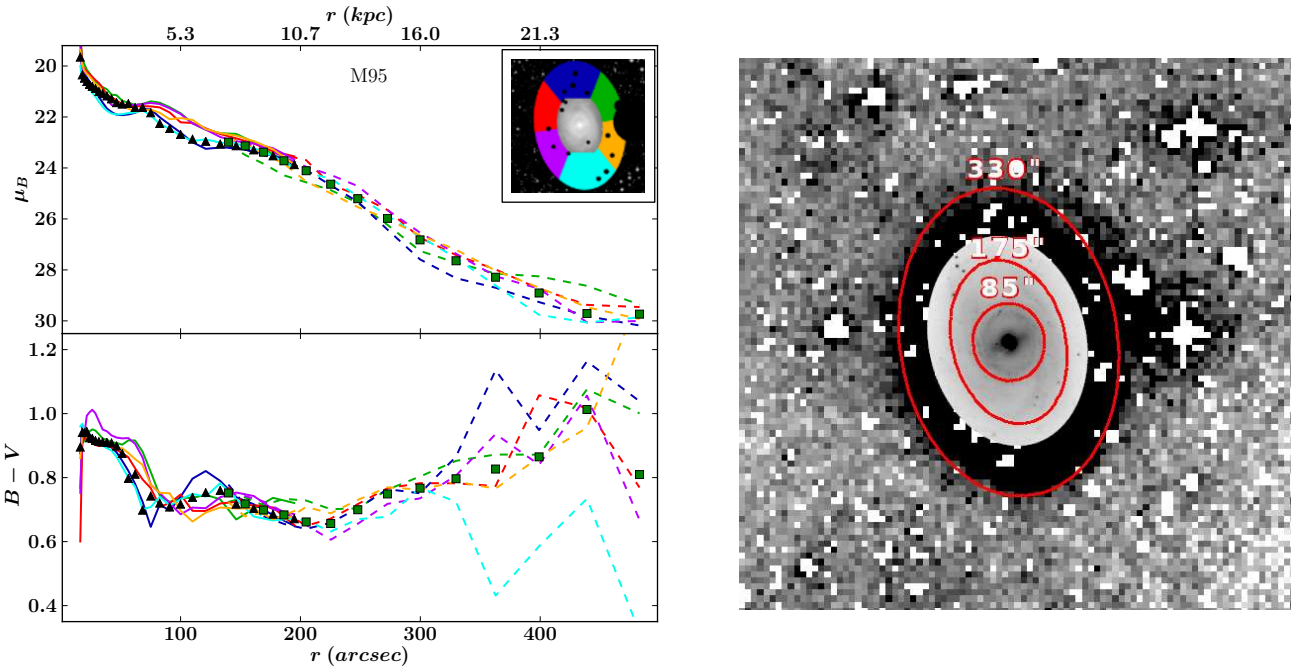

Figure 10. As Figure 6, now for M95. We measure an inner scale length of 64.26″ (3.4 kpc), and an outer scale length of 42.32″ (2.3 kpc) beyond the break at 200″.

the north and 2×10^{-5} $M_\odot$ yr^{-1} kpc^{-2} in the south, a factor of two lower. That said, these derived SFRs do not take into account dust attenuation, which can be a significant factor in deriving SFRs from UV flux due to scattering and absorption effects; Buat et al. (2005), for example, found a mean FUV attenuation of 1.6 magnitudes in their galaxy sample (which was dominated by late-type galaxies). A more detailed analysis of the SFR in M96 should of course take these effects into account.

Nonetheless, this is still apparently fairly low-level star formation that could conceivably be induced by slow accretion from the HI ring, which itself totals only $10^9 M_\odot$. We do also see star formation continuing within the southern arm, so if we assume that this is leftover from the initial accretion where the HI ring meets the galaxy's disk, we can place a lower limit on the timescale of accretion of one orbital time at the 10 kpc radius where we see the spiral arms, which is roughly 400 Myr. This does not seem to pose a problem for the 1.2 Gyr interaction timescale proposed by (Michel-Dansac et al. 2010), or even the 500 Myr timescale proposed by (Rood & Williams 1984) if we assume gas began accreting immediately after the time of the interaction. However, it is also true that the current star formation rate is not high enough to build the outer disk in a reasonable time frame; at this rate, to produce the total disk luminosity beyond 200″ would require longer than a Hubble time. As such, the accretion timescale given here cannot differentiate between a collisional scenario, in which M96 began accreting HI shortly after it had been ejected from NGC 3384, and a non-collisional scenario, in which M96 began accreting HI from a pre-existing cloud 400 Myr ago or earlier by simply passing near it. Given all of these ambiguities, it is important simply to reiterate that we find no *obvious* indications in our data for this galaxy that any particular collisional model is the correct one.

Regarding NGC 3384, the embedded arcs discussed in section 4.2 are unusually broad, but again, they do not appear to be signatures of a major interaction. As stated previously, the symmetric morphology of these features strongly resembles shell systems or caustics formed via minor mergers. Such artifacts can be formed from mergers involving low luminosity disk or spheroidal companions (Quinn 1984; Hernquist & Quinn 1987), or simply from accretion of material from a passing galaxy (Hernquist & Quinn 1987). While it can be difficult to constrain the type of the progenitor from the morphology alone, they reflect better the models of dwarf elliptical disruption shown by Hernquist & Quinn (1988). To conserve phase-space volume, shells formed this way should evolve to become sharper over time (Hernquist & Quinn 1988), so the thickness of the shells may thus imply a rather recent merger (or mergers). Minor mergers are also capable of heating disks (Walker et al. 1995) and leaving behind long-lasting (multiple orbit) warps (Quinn et al. 1993) in outer regions. Also, thick-disk formation models using minor mergers tend to show increasing boxiness with decreasing surface brightness (Villalobos & Helmi 2008), so the presence of such signatures in NGC 3384 again does not immediately imply a major, gas-stripping interaction. The nearest extended tidal feature to the galaxy, feature C in Figures 2 and 3, is not at all aligned with the galaxy's disk, making it unlikely that it constitutes stripped material from NGC 3384. The only HI clearly associated with the galaxy is also ambiguous in nature and origin (Oosterloo et al. 2010). So, once again, we find no particularly clear evidence in favor of any given interaction model based on either of these galaxies' properties.

5.1.2. *The case of M95 and M105: passively evolving systems*

The other large spiral in the group, M95, shows no signs of recent interactions; instead, its appearance is completely consistent with mild secular evolution. The only suggestion of a past interaction is the possible connection with the feature B seen in Figures 2 and 3. Given that this galaxy lies on the outskirts of the group, its undisturbed morphology may sim-

ply be another manifestation of the mechanisms responsible for the morphology-density relation (Oemler 1974; Dressler 1980). It is somewhat intriguing, however, that M95 is apparently not host to any satellites capable of visibly disturbing the isophotes out to 25 kpc (given their smoothness at this radius). Regardless, the galaxy appears to have no connection to the HI ring.

This leaves the elliptical galaxy M105, sitting at the center of the group and surrounded almost perfectly by the HI ring. Yet as our deep imaging shows, it is extremely smooth and relaxed. We find only a marginal detection of any interaction signature, in the form of the faint shell-like structure marked in Figure 7. Considering the plethora of low mass members of this group discovered in the HI (Stierwalt et al. 2009), it is truly remarkable just how unperturbed this galaxy is. If the Leo Ring was generated via strong interactions within the group, it is perplexing that the central galaxy shows no evidence of such an encounter.

Yet given the uncertain nature of the interaction model for forming the Leo Ring, it may be that a more reasonable explanation for the Ring's origin lies with M105 itself. Indeed, extended complexes of neutral hydrogen surrounding normal early type galaxies are not rare (e.g., van Gorkom et al. 1986; Franx et al. 1994; Appleton et al. 1990; Schiminovich et al. 2000; Oosterloo et al. 2007, 2010; Serra et al. 2012). While the original "primordial origin" concept for the Leo Ring argued that the HI is a pristine remnant from the early universe out of which the group members formed, modern galaxy formation models have ellipticals forming hierarchically, through major mergers of smaller objects. This process can be quite messy and, if gas-rich galaxies are involved, can eject a significant amount of HI out of the remnant in the form of extended tidal tails. If this gas could settle into an extended ring, this could place the formation of the Leo Ring at an intermediate age – likely many Gyr ago, given the relaxed state of M105 and lack of any observed tidal features around it. However, this idea still suffers from the problem of longevity (how the Ring can be stable for gigayears given the short group crossing times: Schneider 1985). Additionally, it suffers from an angular momentum argument: gas in merger simulations tends mostly to shock and lose angular momentum, sinking to sub-kpc scales and initiating starbursts, with only a fraction remaining in intermediate scale (similar to Cen A: van Gorkom et al. 1990) disks (e.g. Mihos & Hernquist 1996). It would thus seem extremely difficult to create a 200 kpc diameter ring of low column-density gas in this way.

5.2. *The lack of intragroup light*

Our deep imaging shows no extended diffuse intragroup light within the M96 Group, down to a limit of $\mu_B = 30$ mag arcsec^{-2}, save for a few small low surface brightness streams reminiscent of tidally disrupted dwarfs. These objects aside, the lack of a significant extended IGL component in this group is puzzling. For example, Sommer-Larsen (2006) predicted via group simulations that anywhere from 12% to 45% of the light found in groups should exist in an IGL component by the present day, with a spatially patchy distribution. We do not find anything similar to this in the M96 group. Excluding any undetected diffuse component, the amount of IGL we find constitutes an essentially negligible fraction of the total group light ($< 0.01\%$). Sommer-Larsen (2006) did find that the amount of IGL increases as the group evolves, with the so-called "fossil groups" (as defined by D'Onghia et al. 2005) having suffered the most processing. The M96 Group does not qualify as a fossil group by the D'Onghia et al. (2005) criteria,[10] so it may simply be that the group is not dynamically evolved enough to have generated a substantial amount of intragroup light. However, this conclusion is somewhat at odds with M105's very relaxed state, which suggests that that galaxy, at least, is a well evolved system. An alternative model comes from simulations by Kapferer et al. (2010), which argue that the fraction of intragroup stellar mass (and hence IGL) should *decrease* over time due to low frequency of interactions; new stars form in the galaxies over time, but few new stars are ejected to contribute to the IGL. Even so, these models predict that the intragroup stars still contribute from 3% to 30% of the total group stellar mass, which remains higher than what we find. In general, it seems that the M96 Group simply does not easily fall into either of the paradigms described by Kapferer et al. (2010) and Sommer-Larsen (2006).

Comparing observations to simulations is not always straight-forward, however. For example, the stream-like features found in our imaging data, if indeed part of the M96 Group, have luminosities that fall well below the mass resolution in either the Kapferer et al. (2010) or Sommer-Larsen (2006) models. Furthermore, the brightest galaxies in the Sommer-Larsen (2006) simulations, around which the IGL is centered, are apparently much brighter than M105. Those model galaxies show surface brightnesses of $\mu_B \lesssim 26.5$ at a radius of 39 kpc (see their Figure 3), while M105 is already below $\mu_B = 28$ at this radius. This raises the possibility that the M96 Group simply hosts a correspondingly dimmer IGL halo, however if this is the case, it would be at such low surface brightness that it would not contribute more than a few percent of the total group light, again suggesting a much lower IGL fraction than that predicted by the simulations.

Of course, from the observational perspective, quantitative comparisons to simulations or even to other data depends strongly on how one defines IGL in the first place (good demonstrations of this are shown in Kapferer et al. 2010; Rudick 2010b), as well as how one defines a "group" of galaxies. If, for example, we assume a projected area of the M96 Group of ~ 0.13 Mpc^2 (using a rough radius of 200 kpc; see captions of Figures 2 and 3) and use our constraints on the observed IGL (an upper limit of $\mu_B = 30.1$; the light of the three detected streams is negligible), the upper limit on the diffuse starlight of this group comes to ∼4% of total. If we assume instead that the M96 Group and the M66 Group are a single, larger group (as has been suggested due to their low mutual velocity dispersion and similar distances; see Stierwalt et al. 2009), and that diffuse starlight extends uniformly throughout a circular area encompassing both subgroups (a radius of about 4°, or 800 kpc), the IGL fraction increases to 20%, although it is important to reiterate that these are absolute upper limits: we in fact make no such detection). Including the extended disks or halos of the group galaxies would artificially add light to the IGL, hence the often rather large ranges of such quantities found in the literature.

Given this, it is perhaps more reasonable to compare to other observations of group environments on a more qualitative level. Previous observations of the loose M101 Group showed a similar lack of an extended, diffuse IGL component down to a limiting surface brightness of $\mu_B = 29.5$ (Mi-

[10] namely, that the second brightest galaxy is at least 2 magnitudes fainter than the brightest galaxy; in the M96 Group, all four galaxies are within one magnitude of each other.

hos et al. 2013a). However, observations of compact groups by da Rocha & Mendes de Oliveira (2005) and da Rocha et al. (2008) show smooth envelopes of diffuse light surrounding most of the galaxy groups in their sample. Observations of more massive, even denser environments such as galaxy clusters can show even larger fractions of diffuse intergalactic light (e.g. Adami et al. 2005), so it may simply be that local density plays the largest role.

IHL (intrahalo light) in general is thought to be mostly composed of stars that have been gravitationally stripped from their host galaxies (e.g. Napolitano et al. 2003; Murante et al. 2004; Rudick et al. 2006; Purcell et al. 2007). It is thus reasonable to assume that the two most influential factors in the generation of IHL in any given environment are the strength of interactions and the frequency of interactions. These two factors in turn depend on two physical quantities: mass and density of the cluster or group (mass being essentially a proxy for the number of galaxies; Dressler 1980). For example, the Coma Cluster is one of the densest and most massive clusters in the nearby universe, and the diffuse component of this cluster is dense and bright enough to have been identified in early photographic imaging by Zwicky (1951), although substructure was not detected until much later (Gregg & West 1998; Adami et al. 2005). The Virgo Cluster, by contrast, is less massive and dense than Coma, and hosts a fainter ICL component, again with notable substructure (Mihos et al. 2005; Janowiecki et al. 2010; Rudick et al. 2010a). On the low-mass, high-density end, large fractions of IGL (20%–50%) have been found via imaging compact groups of galaxies (Nishiura et al. 2000; White et al. 2003), but with considerable scatter from group to group (da Rocha & Mendes de Oliveira 2005; da Rocha et al. 2008), and some compact groups having little or no IGL (Aguerri et al. 2006; da Rocha et al. 2008). With fewer galaxies in play, interactions should be less frequent; this implies that the actual fraction of stellar mass that is liberated from host galaxies will depend more strongly on the details of each individual interaction (e.g. relative masses, inclination angles, and velocities of the interacting galaxies; Toomre & Toomre 1972; Negroponte & White 1983), thus giving rise to a higher dispersion in IGL properties.

The M96 Group may thus fit into this picture by occupying the low-mass, low-density regime of galaxy environments. Measuring the total mass of the M96 Group is not trivial, since the entire Leo I Group has considerable substructure spatially and kinematically (e.g. Stierwalt et al. 2009). A simple application of the virial theorem using the the velocity dispersions and harmonic mean radii from Stierwalt et al. (2009) yields masses for the M96 Group in the range of 2–6 $\times 10^{12} M_{\odot}$. Using the calibration between velocity dispersion and group mass given by Yang et al. (2007, their equation 6) gives a rough halo mass of $8 \times 10^{12} M_{\odot}$. While it is highly unlikely that the M96 Group is virialized, it seems clear that the M96 Group is less massive than the mass range of previous loose group studies (typically $10^{13} M_{\odot} - 10^{15} M_{\odot}$; Castro-Rodríguez et al. 2003; Feldmeier et al. 2004; Durrell et al. 2004). These more massive loose groups have low IGL fractions as well (2%), yet still seem to contain a higher fraction than that detected in the M96 Group, or the still less massive M101 Group (Mihos et al. 2013a). We may thus be seeing a continuation of this pattern: lower density and lower masses yield lower IHL fractions.

In this context, the Leo Ring may thus serve as a vital clue regarding the types of dynamics seen in low-mass, loose groups such as M96. This is a rare system in the local universe, in terms of the size and mass of the HI complex. A somewhat similar structure resides in the NGC 5291 complex located 58 Mpc away at the edge of the Abell 3574 cluster, but this HI ring is much more massive and contains a number of large, obviously star-forming clouds (Malphrus et al. 1997; Boquien et al. 2007). As discussed in Section 3, star formation in the Leo Ring is much more subtle: it seems to only amount to the three kpc-scale clumps discovered by (Thilker et al. 2009). Bot et al. (2009) did make a tentative discovery of dust within the Ring, near (but not precisely coincident with) the region labeled 1 in (Thilker et al. 2009).

These discoveries are beneficial, as obtaining a metallicity for the ring would be instrumental in constraining the Ring's origin. Again, however, the analyses of these star-forming clumps by Thilker et al. (2009) and Michel-Dansac et al. (2010) produced conflicting results (1/50 solar metallicity in the former and 1/2 solar in the latter), and Bot et al. (2009) considered their dust detection too uncertain to make any definitive conclusion. The Ring also appears devoid of obvious HII regions (Donahue et al. 1995) and planetary nebulae (Castro-Rodríguez et al. 2003). As such, these very localized star forming regions may be the extent of star formation within the Leo Ring. Other avenues for studying star formation and the stellar content of the Leo Ring include the possibility of deep space-based imaging to search for discrete stellar populations in the Ring, and even deeper ground based searches for diffuse Hα indicative of additional on-going star formation throughout the Ring. Such studies are clearly needed to understand the formation and evolution of this structure, and the galaxy group surrounding it.

6. SUMMARY

We have performed deep ($\mu_{B,\mathrm{lim}} \approx 30$ mag arcsec^{-2}) imaging of the M96 Group in order to search for low surface brightness intragroup light, as well as to study the morphologies and stellar properties of the outer disks and halos of galaxies in the group. We find no diffuse stellar counterpart to the group's 200 kpc diameter HI ring down to $\mu_B = 30.1$, but identify three extremely faint ($\mu_B \sim 29.2$ to 29.9) streamlike features apparently associated with the group. Two of these features may be directly associated with the HI ring, as they show some amount of coincidence with similar-looking features in the distribution of neutral hydrogen.

We constructed surface brightness and color profiles (both azimuthally averaged and in discrete angular wedges) for the group's four most massive galaxies – M105, NGC 3384, M96, and M95 – out to ~25 kpc in each disk galaxy, and out to ~50 kpc in the elliptical M105. We find no evidence of recent disturbance in either M105 or M95, though the latter shows a clear disk truncation and redward color gradient beginning around 12 kpc, possibly due to the effects of radial stellar migration. We also find two arcs embedded in NGC 3384's disk, as well as a strong redward gradient in the outer isophotes reaching old halo-like colors ($B - V \approx 1$), which appears to be associated with the outermost arc. M96 shows mild asymmetry in its extreme outer disk, as well as a color asymmetry apparently reflecting mild star formation likely induced by accretion from the HI ring; no disk break is found in the outer disk out to the extent of our data, possibly indicating that this component of M96 is still being built.

The lack of strong tidal disturbances in the outskirts of the group galaxies, coupled with the absence of significant

starlight associated with the Leo Ring provides some tension for models which rely on recent strong encounters between group galaxies to form the HI ring. The connection between the Ring and the individual galaxies remains unclear; however, further study of the small diffuse structures detected in our imaging may allow for further testing of the various theories proposed to explain the origin of the Ring. Finally, unless the M96 Group has been caught in the very early stages of evolution – unlikely, given the relaxed state of its central elliptical, M105 – the extremely low fraction of intragroup light we measure also places constraints on the ability of groups of this mass and density to act as "pre-processors" for the more commonly seen intracluster light found in massive galaxy clusters.

7. ACKNOWLEDGMENTS

This work has been supported by the National Science Foundation via grants 1108964 (J. C. M.) and 0807873 (J. J. F.) and Research Corporation grant 7732 (J. J. F.). We also thank Tom Oosterloo for the use of his WRST HI data in the construction of Figure 3, and Pat Durrell for many useful discussions. This research made use of NumPy, SciPy (Oliphant 2007), and Matplotlib (Hunter 2007). Figures 6 through 10 made use of Min-Su Shin's (University of Michigan) publicly available code img_scale.py [11].

Facility: CWRU:Schmidt - The Burrell Schmidt of the Warner and Swasey Observatory, Case Western Reserve University

REFERENCES

Adami, C., Slezak, E., Durret, F., Conselice, C. J., Cuillandre, J. C., Gallagher, J. S., Mazure, A., Pelló, R., Picat, J. P., & Ulmer, M. P. 2005, A&A, 429, 39
Aguerri, J. A. L., Castro-Rodríguez, N., Napolitano, N., Arnaboldi, M., & Gerhard, O. 2006, A&A, 457, 771
Alloin, D., & Nieto, J. -L. 1982, A&AS, 50, 491
Appleton, P. N., Pedlar, A., & Wilkinson, A. 1990, ApJ, 357, 426
Arp, H. 1966, Atlas of Peculiar Galaxies (Pasadena, CA: California Institute of Technology)
Atkinson, A. M., Abraham, R. G., & Ferguson, A. M. N. 2013, ApJ, 765, article id. 28
Barbon, R., Benacchio, L., & Capaccioli, M. 1976, A&A, 51, 25
Barnes, J. E. 1989, Nature, 338, 123
Barnes, J. E. 1992, ApJ, 393, 484
Barnes, J. E., & Hernquist, L. 1992, Nature, 360, 715
Barnes, J. E. 2002, MNRAS, 333, 481
Bekki, K., Koribalski, B.S., Ryder, S.D., & Couch, W.J. 2005, MNRAS, 357, L21
Belokurov, V. et al. 2006, ApJ, 654, 897
Berentzen, I., Athanassoula, E., Heller, C. H., & Fricke, K. J. 2003, MNRAS, 341, 343
Boquien, M., Duc, P. -A., Braine, J., Brinks, E., Lisenfeld, U., & Charmandaris, V. 2007, A&A, 467, 93
Bot, C., Helou, G., Latter, W. B., Puget, J., Schneider, S. E., & Terzian, Y. 2009, AJ, 138, 452
Bournaud, F., Combes, F., Jog, C. J., & Puerari, I. 2005, A&A, 438, 507
Bregman, J. N., Hogg, D. E., & Roberts, M. S. 1992, ApJ, 387, 484
Buat, V. et al. 2005, ApJ, 619, L51
Bullock, J. S., & Johnston, K. V. 2005, ApJ, 635, 931
Budzynski, J. M., Koposov, S. E., McCarthy, I. G., & Belokurov, V. 2014, MNRAS, 437, 1362
Burkert, A., Brodie, J., & Larsen, S. 2005, ApJ, 628, 231
Busarello, G., Capaccioli, M., D'Onofrio, M., Longo, G., Richter, G., & Zaggia, S. 1996, A&A, 314, 32
Castro-Rodríguez, N., Aguerri, J. A. L., Arnaboldi, M., Gerhard, O., Freeman, K. C., Napolitano, N. R., & Capaccioli, M. 2003, A&A, 405, 803
Ciardullo, R., Jacoby, G. H., & Dejonghe, H. B. 1993, ApJ, 414, 454
Colina, L., Garcia Vargas, M. L., Mas-Hesse, J. M., Alberdi, A., & Krabbe, A. 1997, ApJ, 484, L41
Comerón, S., Knapen, J. H., Beckman, J. E., Laurikainen, E., Salo, H., Martínez-Valpuesta, I., & Buta, R. J. 2010, MNRAS, 402, 2462
Contini, E., De Lucia, G., Villalobos, Á., & Borgani, S. 2014, MNRAS, 437, 3787
da Rocha, C., & Mendes de Oliveira, C. 2005, MNRAS, 364, 1069
da Rocha, C., Ziegler, B. L., & Mendes de Oliveira, C. 2008, MNRAS, 388, 1433
Davis, M., Efstathiou, G., Frenk, C. S., White, S. D. M. 1985, ApJ, 292, 371
Debattista, V. P., Mayer, L., Carollo, C. M., Moore, B., Wadsley, J., & Quinn, T. 2006, ApJ, 645, 209
de Vaucouleurs, G. 1975, in *Stars and Stellar Systems*, Vol 9, *Galaxies and the Universe*, ed. A. Sandage, M. Sandage, and J. Kristian (Chicago: University of Chicago Press), p. 557
de Vaucouleurs, G., & Capaccioli, M. 1979, ApJS, 40, 699
de Vaucouleurs, G., de Vaucouleurs, A., Corwin, H. G. Jr., Buta, R. J., Paturel, G., & Fouqué, P. 1991, Third Reference Catalogue of Bright Galaxies (Springer(New York))
Devereux, N. A., Kenney, J. D. P., & Young, J. S. 1992, AJ, 103, 784
Donahue, M., Aldering, G., & Stocke, J. T. 1995, ApJ, 450, 45
D'Onghia, E., Sommer-Larsen, J., Romeo, A. D., Burkert, A., Pedersen, K., Portinari, L., & Rasmussen, J. 2005, ApJ, 630, L109
Douglas, N. G., Napolitano, N. R., Romanowsky, A. J., Coccato, L., Kuijken, K., Merrifiedl, M. R., Arnaboldi, M., Gerhard, O., Freeman, K. C., Merrett, H. R., Noordermeer, E., & Capaccioli, M. 2007, ApJ, 664, 257
Dressler, A. 1980, ApJ, 236, 351
Durrell, P. R., Decesar, M. E., Ciardullo, R., Hurley-Keller, D., & Feldmeier, J. J. 2004, Recycling Intergalactic and Interstellar Matter, 217, 90
Elmegreen, D. M., Chromey, F. R., Santos, M., & Marshall, D. 1997, ApJ, 114, 1850
Erwin, P. 2004, A&A, 415, 941
Erwin, P., Pohlen, M., & Beckman, J. E. 2008, AJ, 135, 20
Feitzinger, J. V., & Galinski, T. 1985, A&AS, 61, 503
Feldmeier, J. J., Mihos, J. C., Morrison, H. L., Rodney, S. A., & Harding, P. 2002, ApJ, 575, 587
Feldmeier, J. J., Mihos, J. C., Morrison, H. L., Harding, P., Kaib, N., Dubinski, J. 2004, ApJ, 609, 617
Feldmeier, J. J., Ciardullo, R., Jacoby, G. H., Durrell, P. R., & Mihos, J. C. 2004, Recycling Intergalactic and Interstellar Matter, 217, 64
Forbes, D. A., Beasley, M. A., Bekki, K., Brodie, J. P., & Strader, J. 2003, Science, 301, 1217
Franx, M., van Gorkum, J. H., & de Zeeuw, P. T. 1994, ApJ, 436, 642
Frenk, C. S., White, S. D. M., Davis, M., & Efstathiou, G. 1988, ApJ, 327, 507
Gelb, J. M., & Bertschinger, E. 1994, ApJ, 436, 467
Geller, M. J., & Huchra, J. P. 1983, ApJS, 52, 61
Gerber, R. A., Lamb, S. A., & Balsara, D. S. 1992, ApJ, 399, L51
Gil de Paz, A., Madore, B. F., Boissier, S., Swaters, R., Popescu, C. C., Tuffs, R. J., Sheth, K., Kennicutt, R. C., Jr., Bianchi, L., Thilker, D., & Martin, D. C. 2005, ApJ, 627, L29
Gonzalez, A. H., Zabludoff, A. I., Zaritsky, D., & Dalcanton, J. J. 2000, ApJ, 536, 561
Gonzalez, A. H., Zaritsky, D., & Zubludoff, A. I. 2007, ApJ, 666, 147
Gonzalez, A. H., Sivanandam, S., Zabludoff, A. I., & Zaritsky, D. 2013, ApJ, 778, 14
Goudfrooij, P., Hansen, L., Jørgensen, H .E., Nørgaard-Nielsen, H. U., de Jong, T., & van den Hoek, L. B. 1994, ApJS, 104, 179
Graham et al. 1997, ApJ, 477, 535
Gregg, M. D., & West, M. J. 1998, Nature, 396, 549
Guo, Q., White, S., Boylan-Kolchin, M., et al. 2011, MNRAS, 413, 101
Harris, W. E., Harris, G. L. H., Layden, A. C., & Wehner, E. M. H. 2007, ApJ, 666, 903
Helfer, T. T., Thornley, M. D., Regan, M. W., Wong, T., Sheth, K., Vogel, S. N., Blitz, L., & Bock, D. C. J. 2003, ApJS, 145, 259
Henriques, B. M. B., & Thomas, P. A. 2010, MNRAS, 403, 768
Hernquist, L. & Quinn, P. J. 1987, ApJ, 312, 1
Hernquist, L. & Quinn, P. J. 1988, ApJ, 331, 682
Hernquist, L. 1992, ApJ, 400, 460
Hickson, P., Richstone, D. O., & Turner, E. L. 1977, ApJ, 213, 323
Hodge, P. W. 1971, ARA&A, 9, 35
Høg, E., Fabricius, C., Makarov, V. V., Urban, S., Corbin, T., Wycoff, G., Bastian, U., Schwekendiek, P., & Wicenec, A. 2000, A&A, 355, L27

[11] http://dept.astro.lsa.umich.edu/~msshin/science/code/Python_fits_image/

Hopkins, P. F., Bundy, K., Murray, N., Quataert, E., Lauer, T. R., & Ma, C.-P. 2009, MNRAS, 398, 898
Huchra, J. P., & Geller, M. J. 1982, ApJ, 257, 423
Hunter, J. D. 2007, *Computing in Science & Engineering*, 9, 90
Ivezić, Ž. et al. 2007, AJ, 134, 973
Janowiecki, S., Mihos, J. C., Harding, P., Feldmeier, J. J., Rudick, C., & Morrison, H. 2010, ApJ, 715, 972
Jedrzejewski, R. I. 1987, MNRAS, 226, 747
Jenkins, A., Frenk, C. S., White, S. D. M., Colberg, J. M., Cole, S., & Evrard, A. E. 2001, MNRAS, 321, 372
Kapferer, W., Schindler, S., Knollmann, S. R., & van Kampen, E. 2010, A&A, 516, id.A41
Karachentsev, I. D., Makarov, D. I., & Kaisina, E. I. 2013, AJ, 145, article id. 101
Karachentseva, V. E., & Karachentsev, I. D. 1998, A&AS, 127, 409
Kauffmann, G., Li, C., Fu, J. Saintonge, A., Catinella, B., Tacconi, L. J., Kramer, C., Genzel, R., Moran, S., & Schiminovich, D. 2012, MNRAS, 422, 997
Kennicutt, R. C. 1998, ARA&A, 36, 189
Klypin, A., Kravtsov, A. V., Valenzuela, O., & Prada, F. 1999, ApJ, 522, 82
Kormendy, J., & Kennicutt, R. C. Jr. 2004, ARA&A, 42, 603
Kormendy, J., & Bender, R. 2012, ApJS, 198, 2
Kraljic, K., Bournaud, F., & Martig, M. 2012, ApJ, 757, article id. 60
Krisciunas, K. 1997, Publications of the Astronomical Society of the Pacific, 109, 1181
Landolt, A. U. 1992, AJ, 104, 340
Law, D. R., Johnston, K. V., & Majewski, S. R. 2005, ApJ, 619, 807
Lemonias, J. J. et al. 2011, ApJ, 733, article id. 74
Li, Z., Ho, L. C., Barth, A. J., & Peng, C. Y. 2011, ApJS, 197, 22
Lin, Y.-T., & Mohr, J. J. 2004, ApJ, 617, 879
Lupton, R. H., in SDSS Data Release 8, Transformations Between SDSS Magnitudes and Other Systems, www.sdss3.org/dr8/algorithms/sdssUBVRITransform.php#Lupton2005
Lynden-Bell, D. 1976, MNRAS, 174, 695
Lynds, R. & Toomre, A. 1976, ApJ, 209, 382
Maia, M. A. G., Willmer, C. N. A., & da Costa, L. N. 1998, AJ, 115, 49
Malin, D. F., & Carter, D. 1983, ApJ, 274, 534
Malin, D. F. 1984, in: Astronomy with Schmidt Type Telescopes. IAU Coll. 58. ed. M. Capaccioli (Reidel: Dordrecht). p.73
Malphrus, B. K., Simpson, C. E., Gottesman, S. T., & Hawarden, T. G. 1997, AJ, 114, 142
Martin, D. C. et al. 2005, ApJ, 619, L1
Martínez-Delgado, D., Peñarrubia, J., Gabany, R. J., Trujillo, I., Majewski, S. R., & Pohlen, M. 2008, ApJ, 689, 184
Martínez-Delgado, D., Pohlen, M., Gabany, R. J., Majewski, S. R., Peñarrubia, J., & Palma, C. 2009, ApJ, 692, 955
Martínez-Delgado, D. et al. 2010, AJ, 140, 962
Martín-Navarro, I., Trujillo, I., Knapen, J. H., Bakos, J., & Fliri, J. 2014, submitted (arXiv:1401.3749)
Mateo, M. 1998, ARA&A, 36, 435
Matteucci, F., & François, P. 1989, MNRAS, 239, 885
Mazzei, P., Curir, A., & Bonoli, C. 1995, AJ, 110, 559
McConnachie, A. W. 2012, AJ, 144, article id. 4
McGee, S. L., & Balogh, M. L. 2010, MNRAS, 403, L79
Metz, M., & Kroupa, P. 2007, MNRAS, 376, 387
Meusinger, H., Ismail, H. A., & Notni, P. 2007, Astronomiche Nachrichten, 328, 562
Michel-Dansac, L., Duc, P.- A., Bournaud, F., Cuillandre, J.- C., Emsellem, E., Oosterloo, T., Morganti, R., Serra, P., & Ibata, R. 2010, ApJ, 717, L143
Mihos, J. C., & Hernquist, L. 1996, ApJ, 464, 641
Mihos, J. C. 2004, IAU Symposium Series, 217, 390
Mihos, J. C., Harding, P., Feldmeier, J. J., & Morrison, H. 2005, ApJ, 631, L41
Mihos, J. C., Harding, P., Spengler, C. E., Rudick, C. S., & Feldmeier, J. J. 2013, ApJ, 762, article id. 82
Miville-Deschênes, M. -A., & Lagache, G. 2005, ApJS, 157, 302
Monaco, P., Murante, G., Borgani, S., & Fontanot, F. 2006, ApJ, 652, L89
Moore, B., Ghigna, S., Governato, F., Lake, G., & Quinn, T. 1999, ApJ, 524, L19
Murante, G., Arnaboldi, M., Gerhard, O., Borgani, S., Cheng, L. M., Diaferio, A., Dolag, K., Moscardini, L., Tormen, G., Tornatore, L., & Tozzi, P. 2004, ApJ, 607, L83
Murante, G., Giovalli, M., Gerhard, O., et al. 2007, MNRAS, 377, 2
Naab, T., & Ostriker, J. P. 2006, MNRAS, 366, 899
Napolitano et al. 2003, ApJ, 594, 172
Negroponte, J., & White, S. D. M. 1983, MNRAS, 205, 1009
Nishiura, S., Murayama, T., Shimada, M., et al. 2000, AJ, 120, 2355
Oemler, A. Jr. 1974, ApJ, 194, 1
Oliphant, T. E. 2007, *Computing in Science & Engineering*, 9, 10
Oosterloo, T. A., Morganti, R., Sadler, E. M., van der Hulst, T., & Serra, P. 2007, A&A, 465, 787
Oosterloo, T. A., Morganti, R., Crocker, A., Jütte, E., Cappellari, M., de Zeeuw, T., Krajnović, D., McDermid, R., Kuntschner, H., Sarzi, M., & Weijmans, A.-M. 2010, MNRAS, 409, 500
Pastoriza, M. G., Winge, C., Ferrari, F., Macchetto, F. D., & Caon, N. 2000, ApJ, 529, 866
Patat, F. 2003, A&A, 400, 1183
Pawlowski, M. S., Kroupa, P., Angus, G., de Boer, K. S., Famaey, B., & Hensler, G. 2012, MNRAS, 424, 80
Peñarrubia, J., McConnachie, A., & Babul, A. 2006, ApJ, 650, L33
Pierce, M. J., & Tully, R. B. 1985, AJ, 90, 450
Pinkney, J. et al. 2003, ApJ, 596, 903
Planck Collaboration, Abergel, A. et al. 2013, Submitted
Pohlen, M., Dettmar, R.-J., Lütticke, R., & Aronica, G. 2002, A&A, 392, 807
Pohlen, M., & Trujillo, I. 2006, A&A, 454, 759
Puchwein, E., Springel, V., Sijacki, D., & Dolag, K. 2010, MNRAS, 406, 936
Purcell, C. W., Bullock, J. S., Zentner, A. R. 2007, ApJ, 666, 20
Purcell, C. W., Bullock, J. S., & Zentner, A. R. 2008, MNRAS, 391, 550
Quinn, P. J. 1984, ApJ, 279, 596
Quinn, P. J., Hernquist, L., & Fullagar, D. P. 1993, ApJ, 403, 74
Roberts, M. S., & Haynes, M. P. 1994, ARA&A, 32, 115
Rood, H. J. & Williams, B. A. 1984, ApJ, 285, 5
Roškar, R., Debattista, V. P., Stinson, G. S., Quinn, T. R., Kaufmann, T. & Wadsley, J. 2008, ApJ, 675, L65
Roškar, R., Debattista, V. P., Quinn, T. R., Stinson, G. S., & Wadsley, J. 2008, ApJ, 684, L79
Rudick, C. S., Mihos, J. C., & McBride, C. 2006, ApJ, 648, 936
Rudick, C. S., Mihos, J. C., Frey, L. H., & McBride, C. K. 2009, ApJ, 699, 1518
Rudick, C. S., Mihos, J. C., Harding, P., et al. 2010, ApJ, 720, 569
Rudick, C. S. 2010, ProQuest Dissertations And Theses; Thesis (Ph.D.)–Case Western Reserve University, 2010.; Publication Number: AAT 3425321
Sage, L. J., & Welch, G. A. 2006, ApJ, 644, 850
Sancisi, R., Fraternali, F., Oosterloo, T., & van der Hulst, T. 2008, A&A Rev., 15, 189
Schanberg, B. C. 1973, ApJS, 26, 115
Scheick, S., & Kuhn, J. R. 1994, ApJ, 423, 566
Schiminovich, D., van Gorkum, J. H., Dijkstra, M., Li, Y., Petric, A., van der Hulst, J. M. 2000, Astronomical Society of the Pacific Conferece Series, 240, 864
Schlafly, E. F., & Finkbeiner, D. P. 2011, ApJ, 737, article id. 103
Schneider, S. E., Helou, G., Salpeter, E. E., & Terzian, Y. 1983, ApJ, 273, L1
Schneider, S. E. 1985, ApJ, 288, L33
Schneider, S. E., Salpeter, E. E., & Terzian, Y. 1986, AJ, 91, 13
Schneider, S. E. 1989, ApJ, 343, 94
Schneider, S. E. et al. 1989, AJ, 97, 666
Schombert, J. M., & Wallin, J. F. 1987, AJ, 94, 300
Schweizer, F., & Seitzer, P. 1992, AJ, 104, 1039
Searle, L. & Zinn, R. 1978, ApJ, 225, 357
Sellwood, J. A., & Binney, J. J. 2002, MNRAS, 336, 785
Serra et al. 2012, MNRAS, 422, 1835
Sérsic, J. L., & Pastoriza, M. 1967, PASP, 79, 152
Sil'chenko, O. K., Moiseev, A. V., Afanasiev, V. L., Chavushyan, V. H., & Valdes, J. R. 2003, ApJ, 591, 185
Slater, C. T., Harding, P., & Mihos, J. C. 2009, PASP, 121, 1267
Sofue, Y., & Wakamatsu, K.-I. 1993, PASJ, 45, 529
Sommer-Larsen, J., Romeo, A. D., & Portinari, L. 2005, MNRAS, 357, 478
Sommer-Larsen, J. 2006, MNRAS, 369, 958
Spitzer, L. Jr., & Baade, W. 1951, ApJ, 113, 413
Springel et al. 2005, Nature, 435, 629
Springel, V., Wang, J., Vogelsberger, M., Ludlow, A., Jenkins, A., Helmi, A., Navarro, J. F., Frenk, C. S., White, S. D. M. 2008, MNRAS, 391, 1685
Statler, T. S., & Smecker-Hane, T. 1999, AJ, 117, 839
Stierwalt, S. et al. 2009, AJ, 138, 338
Taranu, D. S., Dubinski, J., & Yee, H. K. C. 2013, ApJ, 778, article id. 61
Thilker, D. A. et al. 2005, ApJ, 619, L79
Thilker, D. A. et al. 2007, ApJS, 173, 538
Thilker, D. A., Donovan, J., Schiminovich, D., Bianchi, L., Boissier, S., Gil de Paz, A., Madore, B. F., Martin, D. C., & Seibert, M. 2009, Nature, 7232, 990

Tomita, A., Aoki, K., Watanabe, M., Takata, T., Ichikawa, S.-I. 2000, AJ, 120, 123
Toomre, A. & Toomre, J. 1972, ApJ, 178, 623
Toomre, A. 1977, in The Evolution of Galaxies and Stellar Populations, ed. B, Tinsley & R. Larson (New Haven: Yale Univ. Press) 401
Trujillo, I., Martinez-Valpuesta, I., Martínez-Delgado, D., Peñarrubia, J., Gabany, R. J., & Pohlen, M. 2009, ApJ, 704, 618
Tully, R. B. 1987, ApJ, 321, 280
Uson, J. M., Boughn, S. P., & Kuhn, J. R. 1991, ApJ, 369, 46
van den Bergh, S. 2008, MNRAS, 390, L51
van der Kruit, P. C. 1979, A&AS, 38, 15
van Dokkum, P. G. et al. 2010, ApJ, 709, 1018
van Gorkom, J. H., Knapp, G. R., Raimond, E., Faber, S. M., & Gallagher, J. S. 1986, AJ, 91, 791
van Gorkom, J. H., van der Hulst, J. M., Haschick, A. D., & Tubbs, A. D. 1990, AJ, 99, 1781
Villalobos, Á., & Helmi, A. 2008, MNRAS, 391, 1806
Walker, I. R., Mihos, J. C., & Hernquist, L. 1996, ApJ, 460, 121
Watson, D. F., Berlind, A. A., & Zentner, A. R. 2012, ApJ, 754, 90
Weisz, D. R. et al. 2011, ApJ, 739, article id. 5
White, S. D. M. & Frenk, C. S. 1991, ApJ, 379, 52
White, P. M., Bothun, G., Guerrero, M. A., West, M. J., & Barkhouse, W. A. 2003, ApJ, 585, 739
Williams, B. F., Delcanton, J. J., Stilp, A., Dolphin, A., Skillman, E. D. & Radburn-Smith, D. 2013, ApJ, 765, article id. 120
Yang, B., Zhu, J., & Song, Y.-Y. 2002, *Chinese Journal of Astronomy and Astrophysics*, 2, 474
Yang, X., Mo, H. J., van den Bosch, F. C., et al. 2007, ApJ, 671, 153
York, D. G. et al. 2000, AJ, 120, 1579
Younger, J. D., Cox, T. J., Seth, A. C., & Hernquist, L. 2007, ApJ, 670, 269
Zibetti, S., White, S. D. M., Schneider, D. P., & Brinkmann, J. 2010, MNRAS, 358, 949
Zwicky, F. 1951, PASP, 63, 61